5-2021

Design of a Cable-Driven Manipulator for Large-Scale Additive Manufacturing

Phillip Chesser
pchesser@vols.utk.edu

To the Graduate Council:

I am submitting herewith a thesis written by Phillip Chesser entitled "Design of a Cable-Driven Manipulator for Large-Scale Additive Manufacturing." I have examined the final electronic copy of this thesis for form and content and recommend that it be accepted in partial fulfillment of the requirements for the degree of Master of Science, with a major in Mechanical Engineering.

William R. Hamel, Major Professor

We have read this thesis and recommend its acceptance:

Mark Noakes, Chad E. Duty

Accepted for the Council:
Dixie L. Thompson

Vice Provost and Dean of the Graduate School

(Original signatures are on file with official student records.)

Design of a Cable-Driven Manipulator for Large-Scale Additive Manufacturing

A Thesis Presented for the

Master of Science

Degree

The University of Tennessee, Knoxville

Phillip Chesser

May 2021

DEDICATION

This work is dedicated to the memory of my father, Joel Chesser, who helped instill in me my passion for engineering, my work ethic, and my love for Christ.

ACKNOWLEDGEMENTS

This work would not have been possible without the whole Oak Ridge National Lab SkyBAAM team including Brian Post, Randall Lind, Peter Lloyd, Alex Boulger, Alex Roschli, Joshua Vaughan, Jesse Heineman, Peter Wang, Celeste Atkins, Matthew Sallas, Nikolaos Tsiamis, Chris Hershey, Emma Betters, and others.

I would like to thank my advisor, Dr. William Hamel, for his support of this thesis.

I would like to thank Randall Lind for his encouragements to pursue graduate studies.

I would like to thank my wife, Elayna, for her patience and encouragement throughout my graduate studies.

ABSTRACT

Additive manufacturing of concrete is a growing field of research, yet current motion platforms do not offer viable routes towards large scale deployable systems. This thesis presents the design and analysis of a novel cable-driven robot for use in large-scale additive manufacturing. The system developed, termed SkyBAAM, is designed to be easily deployable to a construction site for on-site additive manufacturing of buildings and other large structures. The design philosophy behind this system is presented. Analysis of this system first explores the kinematics, and stiffness as a function of cable tension. Analysis of the workspace and singularities is also performed, and scaling laws for the system are examined. A prototype system that was built at ORNL is presented, and data from this system shows is suitability for large-scale printing. In order to scale this out to full-size deployment there are, however, challenges associated with scaling and workspace shape that are identified as targets for future research. However, the success of this system demonstrates the feasibility of cable-driven robots for large, deployable additive manufacturing systems.

TABLE OF CONTENTS

LIST OF TABLES

LIST OF FIGURES

Chapter One

INTRODUCTION

Concrete Additive Manufacturing

From the early days of additive manufacturing (AM), researchers have dreamed of the ability to print buildings and other infrastructure-scale items [1] [2]. It has been theorized that many benefits would arise if buildings could be made with AM, such as increased safety in construction, more efficient use of materials and the ability to fabricate new types of structures [3].

Lind originally proposed the idea in a lab notebook in 1993 and later built a system and published on it [1]. Another early researcher to build a system was Khoshnevis who founded Contour Crafting [4]. More recently, the Chinese company Winsun gained notice for printing concrete houses and office buildings. The U. S. Army Corps of Engineers has been researching the printing of barracks for forward operating bases in recent years [5]. As the idea of printing structures had gained in popularity, NASA has proposed printing future habitats on other planets in their 3D-Printed Habitat Challenge where teams from around the country competed [6]. These are just a few of the groups that are actively researching in this field. Buswell *et al*. [7] and Bos *et al*. [8] have noted the growing number of researchers in concrete AM.

The vision for what could be possible with concrete AM is grand. With the geometric freedom of AM, new types of structures could be fabricated. These could incorporate new and elaborate aesthetic features, bringing exotic architectural features, such as curved walls, within the reach of average construction. New energy efficient features could be included in structures, such as energy storage and self-shading walls [9]. As AM of structures gets more elaborate, pick and place methods could be used to automatically emplace rebar and structural reinforcement, as well as other elements of the structure such as windows, doors, and plumbing and electrical.

To illustrate the potential effect of widespread adoption of concrete AM in the construction industry, consider the following example. Currently houses cost more than the average yearly income of the occupants, while automobiles cost more than an order of magnitude less. Yet, automobiles are significantly more mechanically complex than houses, taking energy from hydrocarbon fuels and converting that to usable energy through controlled micro-explosions, propelling the passengers in a controlled manner to their destination, while safety is ensured through suites of sensors, and even in some cases self-driving capabilities. On the other hand, houses just sit still. The reason for this disparity is that the automotive industry, nearly from its inception, has been heavily reliant on automation which drives cost down, while the construction industry still has very limited automation. The use of AM in construction would significantly increase the automation in this industry, and it can be hoped that this would eventually lead to more affordable housing prices.

However, one thing is common in the work of almost all researchers in the concrete AM field. Namely, they require the use of a gantry robot to move the printhead through space. Using large scale gantries to print large parts on site is rather impractical, however [10]. In order to print something on a gantry-based system the gantry must be larger than the part being printed, meaning that for printing buildings and infrastructure scale items, the gantries must be larger than entire buildings. Fabricating gantries of this size can be quite expensive. Furthermore, deploying machines of this size is impractical. For example, printing a house would require a printer large enough to contain the house, which would have to be moved on-site and set up. Setting up a large steel gantry structure larger than the house itself intuitively does not make sense. Furthermore, setting up such a gantry would require leveling of the site so the gantry could be set up on level ground; it would require transporting large steel members on site, probably with many trucks, and then these members would have to be assembled, most likely with a crane to form the gantry. After fabrication of the house, the gantry would have to be disassembled from around the house, without damaging the house, and transported off site. All of this would likely add substantial cost, making it unlikely that such a scheme would be economical. These

challenges have led a team of researchers at Oak Ridge National Laboratory (ORNL) to explore other possibilities for motion platforms for concrete additive manufacturing.

Cable-Driven Manipulators

A promising alternative to gantry-based motion platforms is cable-driven motion platforms. Cable-driven robots have higher payload-to-weight ratio than other types of systems and offer larger potential workspaces [11] [12]. These are important benefits for designing a large-scale deployable system.

Generally, cable-driven manipulators have a set of fixed cable winders with cables spanning the space in between the winders and the end effector of the manipulator. As the cable winders pay cable in and out, the position of the end effector is manipulated in space. This means that the distance between the actuators of the system and the end effector does not have to be spanned by relatively heavy solid links, but instead is spanned by relatively light cables. For large deployable systems this is helpful. The majority of the system being composed of only light cables means there is far less mass in the system, making transportation easier. Furthermore, large workspaces can be achieved without the use of massive ridged members.

However, the advantages of cable-driven robots do come at costs in other areas. Cables can only carry loads along the direction of their primary axis, and no moments can be reacted through cables. Additionally, cables can only carry loads in tension and not compression. Care must be taken in the design of cable-driven manipulators to make sure that these limitations are accounted for. Furthermore, cable-driven manipulators tend to have lower stiffness than manipulators with ridged links, and gravity induced sagging of cables must be combated.

There are numerous examples of cable-driven manipulators in the literature [11]. One of the classic examples of a cable-driven manipulator is the National institute of Standards and Technology (NIST) RoboCrane [13]. This is essentially a cable-driven inverted Stewart platform with 6 degrees of freedom (DOF). This was a multipurpose system

intended to aid in large scale manufacturing of items such as buildings, airstrips, bridges, and ships, and was designed to have a high payload-to-weight ratio. Figure 1.1 shows NIST's 6 m prototype of the RoboCrane.

Another well-known example of a cable-driven manipulator is the SkyCam [14]. This is used at sporting events to manipulate television cameras over the field. This system clearly has a very large workspace, being capable of spanning an entire football field. The system uses four cables to suspend an end effector over the field and manipulate it in *x*-*y*-*z* space, with rotations being done through an actuated gimbal on the end effector. The system is not fully constrained by the cables, and gravity is needed to help maintain end effector orientation. This is acceptable, because in this application the requirements that are needed are lower than with traditional robotics manipulators. High bandwidth, high stiffness, and high accuracy are not as important here as in a traditional manipulator applications.

Another area where cable-driven manipulators have been used to great effect is in large telescopes. This application shows the tremendous size to which cable-driven manipulators can be taken. One example of this is the 500 m aperture spherical radio telescope (FAST) in the southwest of China [15]. In this system a large cable-driven manipulator is used to move the telescope's radio receiver over an approximately 500 m diameter reflector with an accuracy of about 1 cm. Figure 1.2 shows the FAST under construction. In this figure six towers can be seen from which the cable-driven manipulator is suspended.

PaR Systems developed a well know cable-driven manipulator for demolition and containment work at Chernobyl. [16] This very large system has a workspace longer than a Boeing 777 with a lifting capacity of 50 tons.

While many cable-driven robots have been developed and some researchers have proposed or built systems to additively manufacture parts with cable-driven robots [17] [18] or even lay bricks [19] [20], there has not been in the literature a system proposed to meet the unique characteristics needed for a large-scale deployable cable-driven system for AM. Oak Ridge National Laboratory (ORNL) is engaged in research to develop a cable-driven motion platform specifically designed for additive manufacturing. To this end a cable-

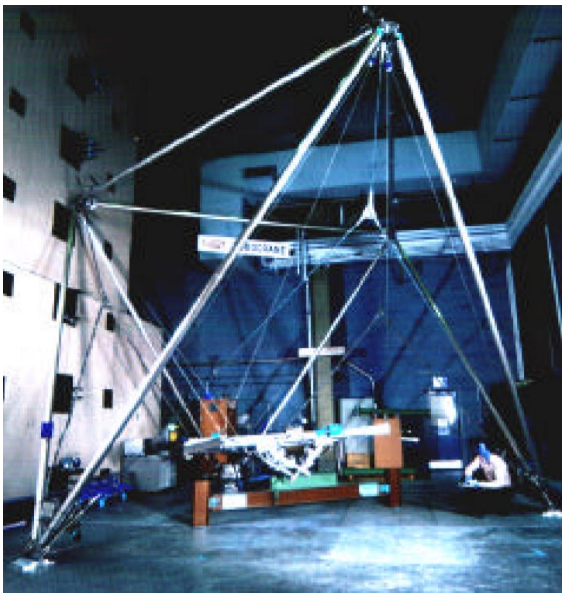

Figure 1.1 6m RoboCrane Prototype [13]

Figure 1.2 FAST Telescope [15]

driven system for AM has been designed and built at ORNL. It is appropriate to note that the system developed in this thesis and built at ORNL has been named Sky Big Area Additive Manufacturing or SkyBAAM. This is a nod towards the cable-driven robot SkyCam, discussed above. From here on the system developed an analyzed in this thesis will be referred to by this name. The SkyBAAM system built at ORNL is meant as a prototype system that will pave the way for potential larger systems in the future.

The aim of this thesis is to develop and analyze a cable configuration that will meet the needs of AM in the construction environment. This will be done in the context of the system developed at ORNL, but potential scaling up to future larger systems will also be investigated. This thesis will proceed in chapter two to develop the system topology of SkyBAAM. In chapter three the system will be modeled, including models of the individual cables and the whole system. Chapter four provides an analysis of the system using these models and looks at system stiffness, singularities, and workspace. This is applied to the system that has been built at ORNL, and scaling laws for future systems are investigated. Chapter five shows the as-built system at ORNL and results from this system. Conclusions, recommendations, and areas of future research are given in chapter six.

Chapter Two
SKYBAAM SYSTEM

There are numerous different cable topologies that have been developed for cable-driven robots over the years [21]. These include, very broadly, cable-driven parallel robots (CDPRs), serial robots, and differential robots. CDPRs have direct connections by cables between the ground and the end effector. Serial and differential cable mechanisms use ridged links connected in a serial manner that are driven by cables. However, the addition of these ridged link detracts from the advantages gained by only having cables to manipulate the end effector. Thus, the configuration chosen for this project is a CDPR.

Furthermore, systems can be fully constrained, over constrained, or under constrained [12]. In under constrained systems, the end effector pose (position and orientation) is not fully defined by the cable positions but is also in part defined by the gravitational load on the end effector. Over constrained systems have the problem that forces on components can inadvertently become very high. Thus, a fully constrained system was chosen for this project. In a fully constrained CDPR there are as many cables controlling the position of the end effector as there are degrees of freedom (DOF). For a three-dimensional system with rotation this is six DOF and six cables.

Having determined that the SkyBAAM system must be a fully constrained CDPR, there is still much flexibility in determining where the cables go and how the cables are kept under tension. Consequently, an understanding of the necessary goals for the system must be developed before proposing cable arrangements.

System Goals

Most cable-driven robots have cable winders at multiple elevated points. In a situation where the robot is permanently installed in a building or high bay, this is not a problem as these winders can be affixed to a large frame or to the building it is housed by. However, in an outdoor fieldable platform this is less practical. Bruckman *et al.* [19] proposed the erection of a large frame around the area where the structure will be fabricated to provide

cable winding points. Gagliardini *et al.* also proposed a reconfigurable CDPR [22]. But this too relied on a large frame that encompassed the workspace. This approach would require significant time and labor to erect a frame that is both large and stiff enough. In fact, this simply reverts to the same problems that are involved in deploying large frames for a gantry robot.

However, some overhead point is necessary to suspend the system above the ground. Instead of a frame supporting many overhead points, a crane can be used to support a single overhead point.

Each piece of cable winding equipment that must be used in the system adds additional equipment that must be deployed, adding the cost of both the system and the deployment. Thus, it is desirable to have the cable winding locations concentrated together into as few winding points as possible. These winding points can be fieldable base stations that are, for example, on trailers that can be driven out onto the jobsite.

The purpose of a motion platform in AM is to constrain and move the deposition head in space. A deposition head in space has three rotational DOF and three translational DOF. In many AM applications the deposition head only needs to be moved in the three translational DOF while the rotational DOF can be fixed. The kinematic arraignment of a motion platform for AM should be able to manipulate the deposition head in the translational DOF while constraining the rotational DOF, without over-constraint. As mentioned before, some cable-driven manipulators under constrain the end effector, but since accuracy of the deposition head in space is important, exact constraint of the end effector was chosen.

Furthermore, stiffness of the system is important in order to accurately control the deposition head. Since most AM processes are done in a layer-wise fashion, most motion is in the ground, or x-y, plane. Thus, stiffness in the x-y plane should be prioritized over stiffness in the z direction.

To summarize, the goals of the kinematic arrangement of the cable-driven system are as follows:

1. Single aerial winder
2. Concentrate cable winders in the a few base stations
3. Control translational DOF
4. Remove rotational DOF without over-constraint.
5. Prioritize stiffness in *x*-*y* plane

With these goals in mind the cable configuration can be developed.

Developing the Cable Configuration

To fully and exactly constrain the deposition head in six DOF space, six cables must constrain the motion. The cables used to control motion of the end effector must originate from several fixed winders, one of which is elevated, to meet objectives 1 and 2. Most base stations will have more than one cable going from a winder to the end effector.

A system with six cables each of independently variable lengths can move in six DOF. In order to meet objectives 3 and 4, and control translational motion while removing rotational motion, constraints must be introduced. Liu, Gosslin and Laliberté proposed a method to remove unwanted DOF [23]. Their method resulted in a complex arrangement of springs and pulleys. However, a mechanically simpler method is used here. By constraining some sets of cables to have identical lengths and leveraging parallelogram geometry, rotational DOFs can easily be removed.

For every cable that is constrained and made identical in length to another cable, one DOF is removed. So, if two cables are constrained to have the same length, one DOF is removed. Furthermore, if three different cables have the same length, two more DOF are removed. Thus, a system of six cables where there is a set of both two and three cables that respectively have the same length, then three DOF will be removed from the original six to give a system with three DOF, with the generalized coordinates being the independently

variable lengths. In order to ensure that the removed DOFs are rotational each set of identical length cables must for a parallelogram.

To illustrate this concept, consider the simpler 2D case shown in Figure 2.1. In *a)* there are three non-parallel cables of variable length. A force, F, from a spring keeps the cables under tension so they behave like ridged links. This system can move in three DOFs, two translational and one rotational, as the cable lengths change. If cable 2 is constrained to have the same length as cable 3, then the system will have only two DOFs represented by two generalized coordinates, namely the lengths of cables 1 and 3. However, it is not readily apparent how the system will move, and both DOFs will involve coupled translation and rotation. Next consider case *b)*. Here cables 1 and 2 are both parallel and of the same length. Again, a tension force ensures they behave like rigid links. Now the orientation is constrained, and the system can only move translationally as the cable lengths change. In the full three-dimensional case of a ridged body deposition head in space there are three rotational DOFs that need constrained. Hence a total of three cables that have their lengths constrained to another cable. To create these length constraints, multiple cables that come to the same base station can be wound on the same winding drum. There is only one way to divide cables among base stations to meet this length constraint in this way. Namely, there are three base stations that control motion, and all cables coming from a given base station have cables of equal length that are wound on the same drum; one station will have one cable, one will have two cables and the last will have three cables. With these requirements on the base stations, two concepts were put forth during the design process.

Figure 2.2 shows one of these concepts. The deposition head is shown in red. There are two ground base stations that control motion. These are shown in blue. A platform, shown in yellow, is suspended from a crane and has the final motion cable winder. To keep this platform fixed in space, six stay cables, shown as blue, anchor it to the ground. These six cables fully constrain this platform and prevent motion. The crane that holds this platform only needs to provide an upward force against the stay cables and does not have to rigidly position it. In fact, to prevent over constraint by the crane the connection between the crane and the platform should be compliant.

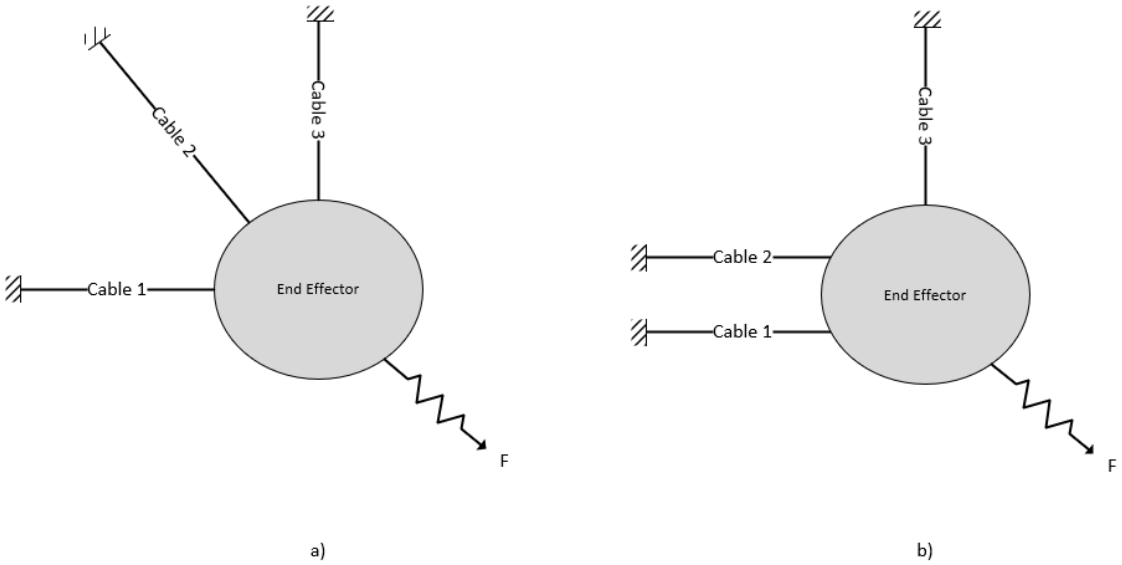

Figure 2.1 2D Cable Constraints

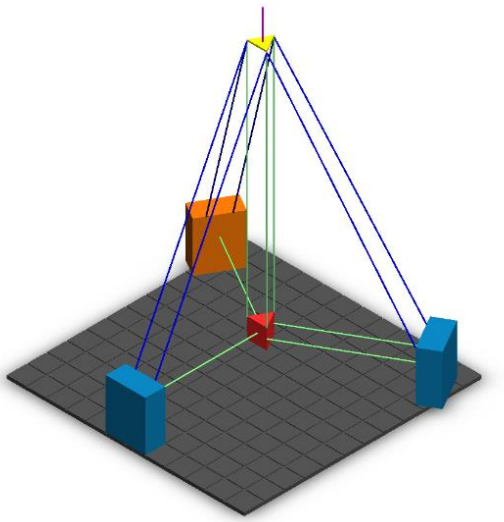

Figure 2.2 Initial SkyBAAM Cable Configuration

For the system to function properly, all the cables must be kept under tension. To ensure this, a tension station is added, shown in orange. The cable that comes from the tension station is controlled with a force control loop. The intention is that this cable does not affect position of the end effector, but only provides a force to pull against the other cables. Since the tension cable is controlled to maintain a given force, the addition of this cables does not over constrain the motion of the system.

Figure 2.3 shows the second concept. In order to meet objective 5 of prioritizing stiffness in the *x*-*y* plane, the cables were rearraigned between the base stations. Here the ground stations have two and three cables respectively while the suspended station has only one cable. This puts the direction of all but one cable primarily in the *x*-*y* plane. Thus, there are more cables contributing to the *x*-*y* stiffness. An additional benefit is that a platform does not have to be suspended. Instead a single pulley can be suspended which the vertical cable can go over to be controlled from a winder on the ground. If this pulley is approximated as a point, instead of a rigid body as with the platform above, only three stay cables are necessary to fix it in space. Again, the connection to the crane should be compliant.

A further improvement with this concept is the addition of a second tension station. With this addition, it is possible to have some control over the net tension vector provided to the end effector. The use of two tension stations was previously proposed by Oh and Agrawal [24] to control system tension, and later in this thesis their methods for controlling tension forms the basis for tension control in SkyBAAM.

These stations are named as shown in Figure 2.3. The station whose cables run primarily in the *x* direction is termed the *x*-station. The tension station opposing the *x*-station is termed the *x'*-station. Naming for *y* and *y'* is similar. The *z*-cable provides primarily the vertical motion. The *z*-cable runs over the suspended pulley and to the *z*-winder on the ground, this pulley being termed the apex.

This second concept both simplifies the system mechanically, and prioritizes stiffness in the *x*-*y* plane when compared to the first concept. For this reason, this kinematic arrangement was selected for the SkyBAAM system.

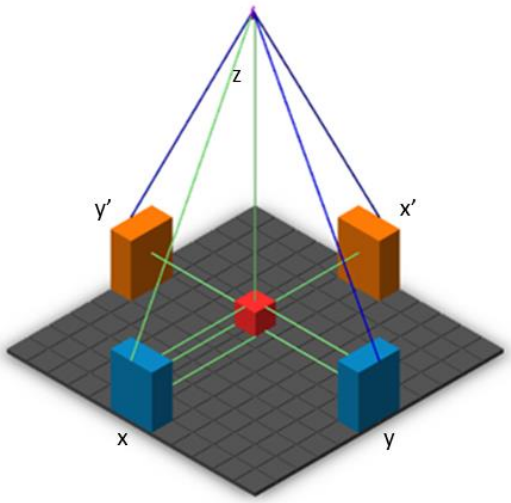

Figure 2.3 Final SkyBAAM Cable Configuration

Summary

In this chapter the goals necessary for a fieldable cable-driven robotic platform for additive manufacturing construction were discussed. This then led to a discussion on possible cable configurations with one selected based on qualitative argumentation. In the next chapter this configuration will be mathematically modeled.

Chapter Three
MODELING SKYBAAM

In this section a mathematical model for SkyBAAM will be developed. This will include deriving a model for the stiffness of the system in order to understand system performance. Also, the forward and inverse kinematics will be derived for use in control of the system. In chapter four the SkyBAAM model will be used evaluate the SkyBAAM system in order to understand the workspace and stiffness of the system. Further understanding of the system will be gained in chapter five with the measured accuracy of the system.

Nomenclature and Definitions

Before proceeding to develop a model of the system a clear set of nomenclature must be developed for the system.

Figure 3.1 shows a diagram of the system. The coordinate system *O* is a fixed coordinate system. The *x*-*y* plane of this coordinate system is parallel to the ground, and *z* points up. A coordinate system *O'* is fixed to the end effector. For convenience, the location of this coordinate system is at the deposition point of the extruder. Because the end effector does not rotate, *x'*, *y'*, and *z'* are parallel to *x*, *y*, and *z*.

As discussed in the previous chapter, there are eight cables of variable length, each with one end grounded to a fixed cable winder and the other end connected to the end effector. These are divided into six that control motion and two that control tension. These will be termed hereafter "motion cables" and "tension cables" respectively. Also as discussed in the previous chapter, the motion cables are divided into three *x*-cables, two *y*-cables, and one *z*-cable. The tensions cable opposing the *x*-cables will be termed the *x'*-cable, while the tension cable opposing the *y*-cables will be termed the *y'*-cable. The cables will be given numbers in the following manner: 1-3 are the *x*-cables, 2-5 are the *y*-cables, 6 is the *z*-cable, 7 is the *x'*-cable and 8 is the *y'*-cable.

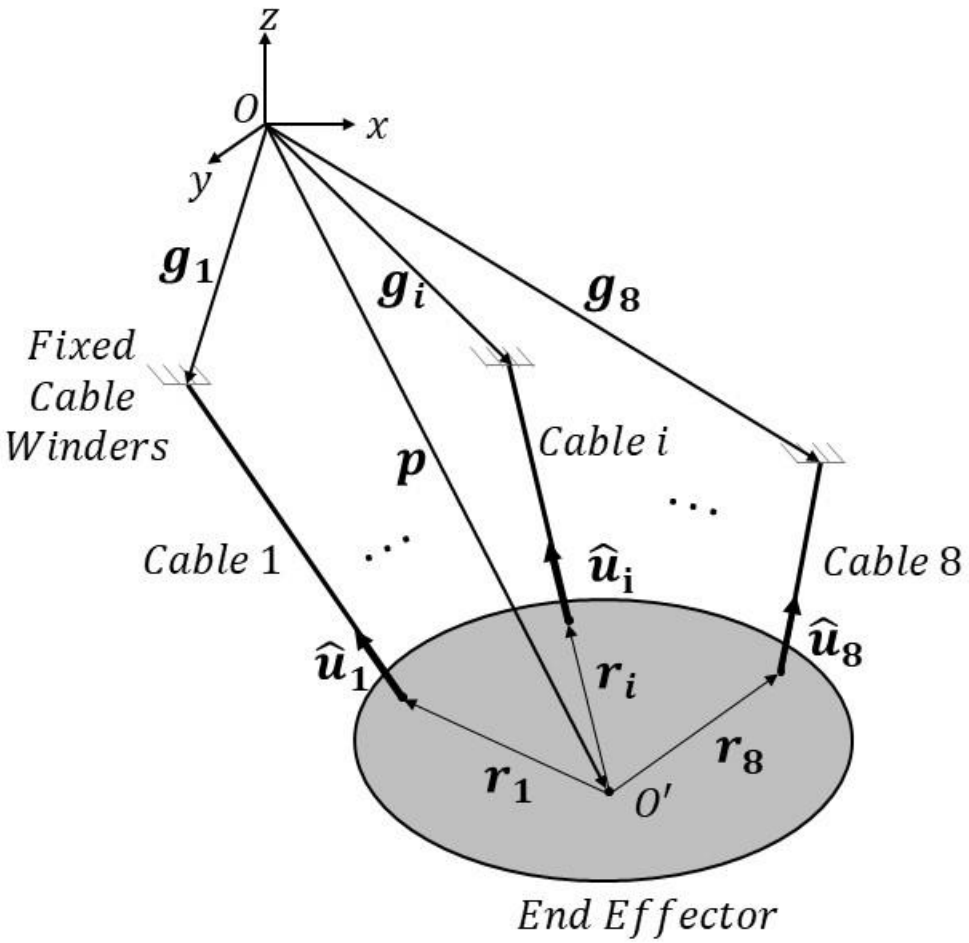

Figure 3.1 SkyBAAM Nomenclature Diagram

The vectors $\boldsymbol{g_1}$ through $\boldsymbol{g_8}$ represent the locations of the cable pick off points with respect to *O*. The vector $\boldsymbol{p}$ represents the location of *O'* relative to *O*. Because of the choice *O'*, this is also the location of deposition in *O*. The vectors $\boldsymbol{r_1}$ through $\boldsymbol{r_8}$ represent the connection points of the cables onto the end effector in *O'*. The vectors $\boldsymbol{\hat{u}_1}$ through $\boldsymbol{\hat{u}_8}$ represent unit vectors along the cables pointing from the end effector to the cable winders in *O'*. With these definitions in place the model of the system can be developed.

Single Cable Model

In a CDPR, the performance of individual cables must be understood to accurately understand the whole system. Thus, modeling of the SkyBAAM system will start with modeling of an individual cable. The effect of gravity causing the cables to sag will be investigated and its effect on stiffness. The implications of this will affect the use of cables within the system.

Catenary Stiffness

The stiffness of a cable, as seen by the end effector, is more than simply the elastic stiffness of the cable. It is also a function the sagging of the cable under gravity. A horizontal cable span under gravity takes the well-known shape of a catenary. The shape and length of a catenary cable are well understood. However, more important for the SkyBAAM is the stiffness implications of a catenary sagging cable.

As a sagging cable is pulled on, the cable will sag less causing the straight-line distance to increase. This gives a compliance to the system, even if the cable itself is completely inelastic. This compliance will be described with what will be called catenary stiffness, k_{cat}. This can then be combined with the elastic stiffness of the cable to give the composite, or total, stiffness of a cable.

In the SkyBAAM system, the *x*, *y*, and tension cables will be close to horizontal with respect to gravity, while the *z*-cable is close to vertical. To simplify the analysis, all but the *z*-cable will be assumed to be horizontal. Even though this is not actually true, it will be considered to be a valid simplifying assumption for two reasons. First, the angle of the *x*

and *y*-cables to the horizontal is small during normal operation. Second, the horizontal assumption is a worst-case scenario. If the direction of one of the cables is slightly in vertical direction, then it will sag less. Thus, the horizontal assumption gives a worst-case bounding scenario. Figure 3.2 shows a diagram of a horizontal, sagging cable.

The length of a purely horizontal catenary cable is given in [25] by:

$$S = 2a * \sinh\frac{\ell}{2a} \tag{3.1}$$

Where S = cable length, ℓ = straight-line distance, t = straight-line force or tension, w = cable weight per unit length, and $a = \frac{t}{w}$.

Equation (3.1) can be simplified with a two term Taylor Series approximation. This is basically a linearization at a point. The Taylor Series approximation will be taken about $\frac{\ell}{2a} = 0$ since this will become more accurate as tension in the cable gets higher. The two term Taylor Series expansion of the hyperbolic sine at $x = 0$ is:

$$\sinh x \cong x + \frac{x^3}{6} \tag{3.2}$$

Substituting the series expansion into (3.1) yields the following expression for cable length:

$$S \cong 2a\left(\frac{\ell}{2a} + \frac{\ell^3}{48a^3}\right) = \ell + \frac{\ell^3 w^2}{24t^2} \tag{3.3}$$

This can be solved for the straight-line tension on the cable:

$$t = \frac{\ell^{3}/_{2}w}{2\sqrt{6}\sqrt{S-\ell}} \tag{3.4}$$

Stiffness is defined as the partial derivative of force with respect to distance. Taking the partial derivative of (3.4) to find stiffness yields:

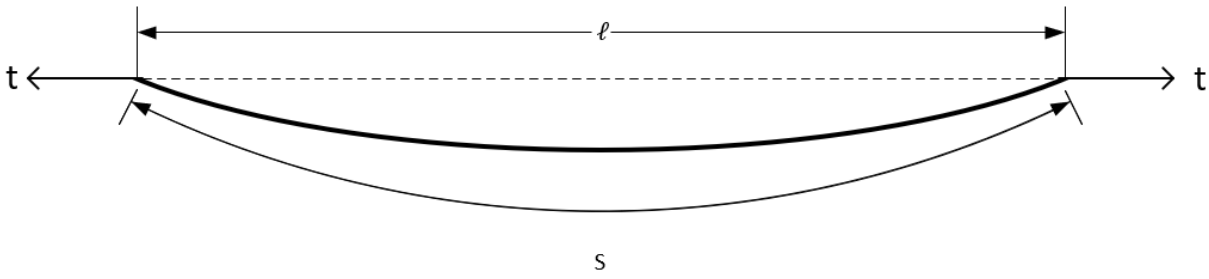

Figure 3.2 Catenary Sag in a Cable

$$k_{cat} = \frac{\partial t}{\partial \ell} = \frac{\partial}{\partial \ell}\left(\frac{\ell^{3}/_{2} w}{2\sqrt{6}\sqrt{S-\ell}}\right) \tag{3.5}$$

If the Taylor Series approximation for S in (3.3) is substituted into (3.5), this simplifies to:

$$k_{cat} = \frac{3t\ell^2 w^2 + 24t^3}{2\ell^3 w^2} = \frac{3t}{2\ell} + \frac{12t^3}{\ell^3 w^2} \tag{3.6}$$

Elastic Stiffness

In addition to the cable sag giving rise to compliance, the cable itself will stretch under tension. This elastic stretching will be described by an elastic stiffness, k_{elas}.

Loos & Co., a cable manufacturer, describes the cable stretch in [23] with the following equation.

$$\%Stretch = \frac{tG}{D^2} \tag{3.7}$$

Where, t = tension on cable, D = cable diameter, and G is a table look up value that depends on the type of cable weave. Putting this in terms of engineering strain yields:

$$\varepsilon = \frac{tG}{100D^2} \tag{3.8}$$

The definition of stress is given by:

$$\sigma = E\varepsilon \tag{3.9}$$

Where E is the modulus of elasticity.

When the stress in a member is caused by an axial load, t, on a cross section, as is the case in a cable, this becomes:

$$\frac{t}{A} = E\varepsilon \tag{3.10}$$

Where A is the area of the cross section.

Substituting in (3.8) and solving for E yields:

$$E = \frac{t}{A\varepsilon} = 100\frac{D^2}{GA} \tag{3.11}$$

Axial stiffness of a member is defined as:

$$k_{elas} = \frac{AE}{\ell} \tag{3.12}$$

Substituting in (3.11) yields:

$$k_{elas} = 100\frac{D^2}{G\ell} \tag{3.13}$$

The value of *G* can then be substituted in depending on the type of wire rope that is used. Loos & Co. tabulated data for *G* for different cable types and materials that are repeated in Table 3.1 [26]. These *G* values are valid for cable diameter and length in inches.

For example, for galvanized 7x19 steel wire rope, *G* = .000014, and so the elastic stiffness becomes:

$$k_{elas} = 7142857.1\frac{D^2}{\ell} \tag{3.14}$$

Composite Stiffness and Implications

The composite stiffness of a cable in a CDPM is a function of both the catenary stiffness and the elastic stiffness of the cable. The composite stiffness of the sagging cable can be represented as an elastic spring and a catenary spring in series as shown in Figure 3.3. A series model for springs is valid when both springs see the same force. Both the catenary and elastic deflections are functions of the same cable tension. Thus, a series model is valid to add the elastic and catenary stiffnesses.

Adding these as series springs yields:

$$k_{net} = \frac{1}{1/k_{elas} + 1/k_{cat}} \tag{3.15}$$

Table 3.1 *G* values for different wire rope types [26]

Cable/Wire Rope Type	G
1x7 302/304 SST	.00000735
1x19 302/304 SST	.00000779
7x7 302/304 SST	.0000120
7x19 302/304 SST	.0000162
6x19 302/304 SST IWRC	.0000157
6x25 302/304 SST IWRC	.0000160
19x7 302/304 SST	.0000197
1x7 Galvanized	.00000661
1x19 Galvanized	.00000698
7x7 Galvanized	.0000107
7x19 Galvanized	.0000140
6x19 Galvanized IWRC	.0000136
6x25 Galvanized IWRC	.0000144
19x7 Galvanized	.0000178
1x7 Galvanized	.00000661

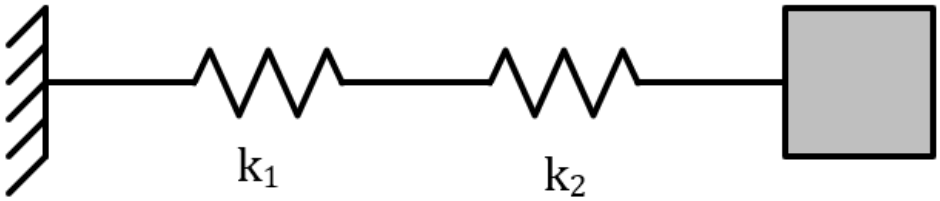

Figure 3.3 Series Springs

Substituting in (3.6) and (3.13) and simplifying yields the following:

$$k_{net} = \frac{300D^2(\ell^2 w^2 t + 8t^3)}{24G\ell t^3 + \ell^3 w^2(200D^2\ell + 3Gt)} \tag{3.16}$$

This expression can then be used for a given cable type, diameter, and length to show how the cable stiffness varies with tension. An example is plotted in Figure 3.4 for a 1/8th inch 7x19 steel wire rope that is 20 feet long. It can be seen in this figure that the stiffness starts at 0 lb/in for no tension and increases asymptotically towards a maximum value as tension increases. This physically makes sense. At first the cable is completely slack, and it takes no force to deflect the cable end. As the tension increases, the sag in the cable deceases. As this happens, it takes more force to axially deflect the end of the cable and it becomes stiffer. To find the maximum stiffness value for a cable, the limit can be taken as the tension becomes infinite.

$$\lim_{t\to\infty} \frac{300D^2(\ell^2 w^2 t + 8t^3)}{24G\ell t^3 + \ell^3 w^2(200D^2\ell + 3Gt)} = 100\frac{D^2}{G\ell} \tag{3.17}$$

It will be noted that this limiting value is the same as the elastic stiffness of the cable. This physically makes sense. As the cable tension tends towards infinity, the cable tends towards becoming perfectly straight. When the cable is perfectly straight the catenary sag no longer plays any part in the stiffness of the cable, and only the elastic stiffness plays a part in the cable stiffness. While cable tension can never be infinite in reality, at high tensions the elastic stiffness dominates in the composite stiffness of the cable, and the catenary effect becomes negligible.

This leads to an important observation. At low tensions the sag dominates the cable stiffness, causing stiffness to be low and leading to significant variation of stiffness with tension. However, at high tensions the elastic stiffness dominates, and the stiffness reaches a higher value, and becomes nearly constant with changing tension.

The system will perform better if the cables are kept in the elastic dominated region. There are several reasons for this. First, this is the highest stiffness range of the cable. This will

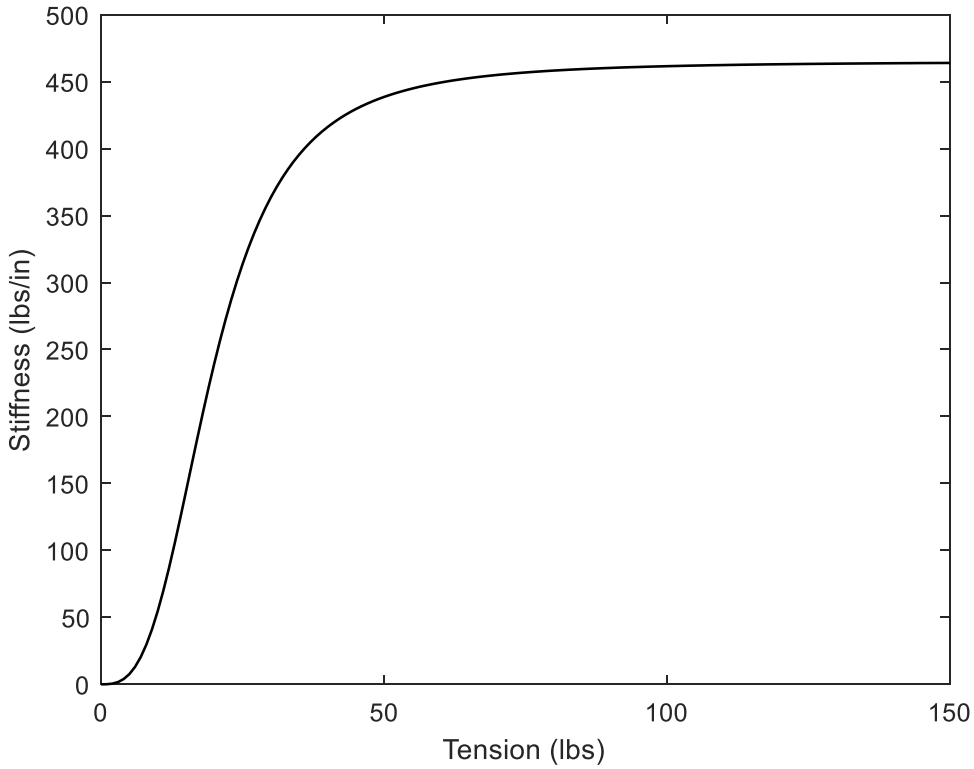

Figure 3.4 Stiffness of 1/8” 7x19 steel wire rope 20’ long

lead to a stiffer end effector and improved system performance. Secondly, a constant stiffness is desirable for linear behavior of this system. This will make control of the system easier. Later in the chapter a method will be developed to ensure that all the cables in the system are kept above a minimum tension to keep them in this elastic region.

System Model

With this preliminary understanding of the behavior of individual cables, a model of the whole system will be developed. First the inverse and forward kinematics will be solved.

Inverse Kinematics

The inverse kinematics of a system will give a mapping from end effector position in Cartesian space to joint positions.

For convenience, Figure 3.5 is a repeat of the system diagram. Here, only the six motion cables will be considered, since the tension cables do not contribute to the motion of the system. The effect of the tension cables will be considered later.

The goal of the inverse kinematics is to find the joint positions (cable lengths) for a given end effector position. With a CDPM the joint positions are simply the cable lengths. Thus, finding the cable lengths for a given end effector position solves the inverse kinematics problem.

The vector that represents cable *i* starts at the terminus of $\boldsymbol{r}_i$, and ends at the terminus of $\boldsymbol{g}_i$. The length of a vector from $\boldsymbol{r}_i$ to $\boldsymbol{g}_i$ is given by:

$$\ell_i = \|\boldsymbol{p} + \boldsymbol{r}_i - \boldsymbol{g}_i\| \tag{3.18}$$

Where $\|\boldsymbol{x}\|$ represents the Euclidean norm of $\boldsymbol{x}$.

Because of the unique geometry of SkyBAAM, $\ell_1 = \ell_2 = \ell_3$, and $\ell_4 = \ell_5$. Thus, the inverse kinematics can be completed by only finding ℓ_1, ℓ_4 and ℓ_6. This will give the lengths of all the motion cables.

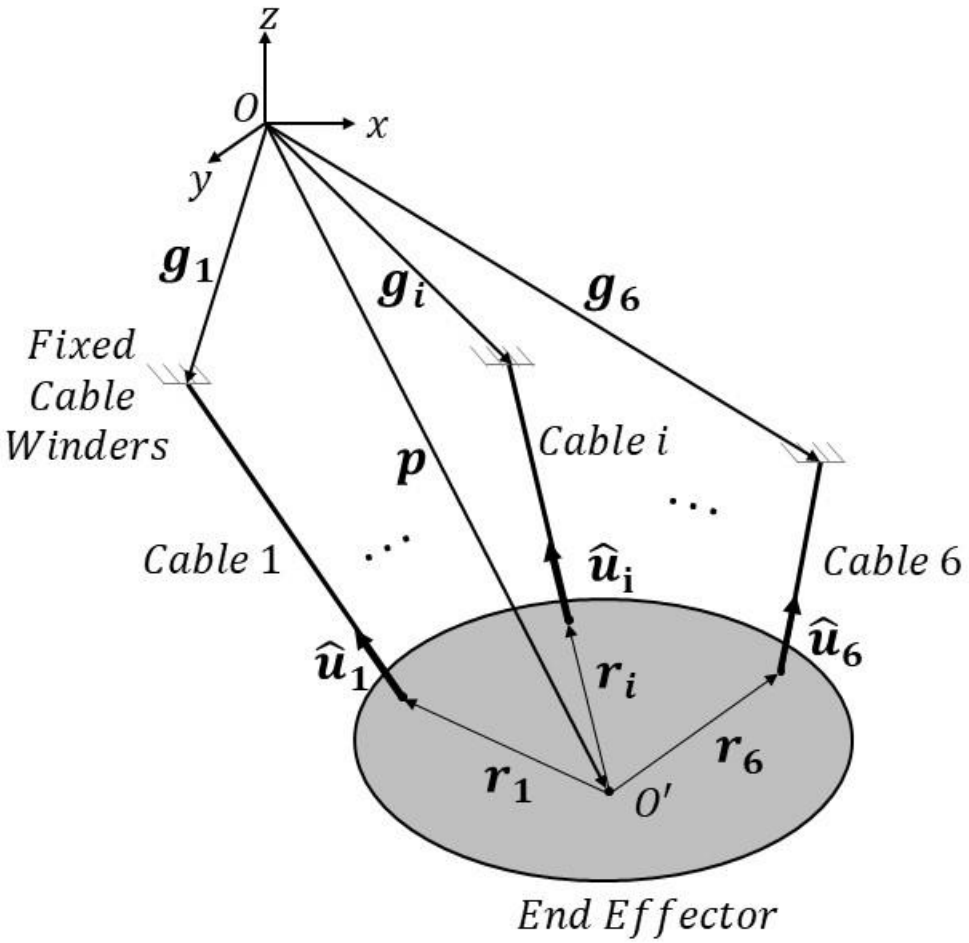

Figure 3.5 SkyBAAM Diagram

Forward Kinematics

Solving the forward kinematics is the opposite problem from the inverse kinematics. Here the joint positions, or cable lengths are known, and the end effector location must be found. For this system the forward kinematics are more involved. Since $\ell_1 = \ell_2 = \ell_3$, and $\ell_4 = \ell_5$ the forward kinematics are fully defined using ℓ_1, ℓ_4 and ℓ_6.

Three equations can be written from (3.18) using the lengths of cables 1, 4 and 6. This gives three simultaneous non-linear equations where $\boldsymbol{p}$ is the unknown location of the end effector in global coordinates. Because the rotation is constrained, the vector $\boldsymbol{p}$ only contains the *x*, *y*, *z* coordinates of the end effector and not the rotational components.

$$\|\boldsymbol{p} + \boldsymbol{r}_1 - \boldsymbol{g}_1\| = \ell_1 \tag{3.19}$$

$$\|\boldsymbol{p} + \boldsymbol{r}_4 - \boldsymbol{g}_4\| = \ell_4 \tag{3.20}$$

$$\|\boldsymbol{p} + \boldsymbol{r}_6 - \boldsymbol{g}_6\| = \ell_6 \tag{3.21}$$

Expanding the Euclidean norms yields**:**

$$\sqrt{(\mathrm{p_x} + \mathrm{r_{1x}} - \mathrm{g_{1x}})^2 + (\mathrm{p_y} + \mathrm{r_{1y}} - \mathrm{g_{1y}})^2 + (\mathrm{p_z} + \mathrm{r_{1z}} - \mathrm{g_{1z}})^2} = \ell_1 \tag{3.22}$$

$$\sqrt{(\mathrm{p_x} + \mathrm{r_{4x}} - \mathrm{g_{4x}})^2 + (\mathrm{p_y} + \mathrm{r_{4y}} - \mathrm{g_{4y}})^2 + (\mathrm{p_z} + \mathrm{r_{4z}} - \mathrm{g_{4z}})^2} = \ell_4 \tag{3.23}$$

$$\sqrt{(\mathrm{p_x} + \mathrm{r_{6x}} - \mathrm{g_{6x}})^2 + (\mathrm{p_y} + \mathrm{r_{6y}} - \mathrm{g_{6y}})^2 + (\mathrm{p_z} + \mathrm{r_{6z}} - \mathrm{g_{6z}})^2} = \ell_6 \tag{3.24}$$

Squaring both sides and multiplying out:

$$p_x^2 + 2p_x(r_{1x} - g_{1x}) + (r_{1x} - g_{1x})^2 + p_y^2 + 2p_y\big(r_{1y} - g_{1y}\big) + \big(r_{1y} - g_{1y}\big)^2 + p_z^2 + 2p_z(r_{1z} - g_{1z}) + (r_{1z} - g_{1z})^2 = {\ell_1}^2 \tag{3.25}$$

$$p_x^2 + 2p_x(r_{4x} - g_{4x}) + (r_{4x} - g_{4x})^2 + p_y^2 + 2p_y\left(r_{4y} - g_{4y}\right) + \left(r_{4y} - g_{4y}\right)^2 + p_z^2 + 2p_z(r_{4z} - g_{4z}) + (r_{4z} - g_{4z})^2 = {\ell_4}^2 \quad (3.26)$$

$$p_x^2 + 2p_x(r_{6x} - g_{6x}) + (r_{6x} - g_{6x})^2 + p_y^2 + 2p_y\left(r_{6y} - g_{6y}\right) + \left(r_{6y} - g_{6y}\right)^2 + p_z^2 + 2p_z(r_{6z} - g_{6z}) + (r_{6z} - g_{6z})^2 = {\ell_6}^2 \quad (3.27)$$

This can be written more compactly by introducing new coefficients:

$${p_x}^2 + 2a_1p_x + {p_y}^2 + 2b_1p_y + {p_z}^2 + 2c_1p_z = d_1 \quad (3.28)$$

$${p_x}^2 + 2a_2p_x + {p_y}^2 + 2b_2p_y + {p_z}^2 + 2c_2p_z = d_2 \quad (3.29)$$

$${p_x}^2 + 2a_3p_x + {p_y}^2 + 2b_3p_y + {p_z}^2 + 2c_3p_z = d_3 \quad (3.30)$$

Where:

$a_1 = (r_{1x} - g_{1x})$ $\quad b_1(r_{1y} - g_{1y})$ $\quad c_1 = (r_{1z} - g_{1z})$

$d_1 = {\ell_1}^2 - {a_1}^2 - {b_1}^2 - {c_1}^2$

$a_2 = (r_{4x} - g_{4x})$ $\quad b_2 = \left(r_{4y} - g_{4y}\right)$ $\quad c_2 = (r_{4z} - g_{4z})$

$d_2 = {\ell_4}^2 - {a_2}^2 - {b_2}^2 - {c_2}^2$

$a_3 = (r_{6x} - g_{6x})$ $\quad b_3 = (r_{6y} - g_{6y})$ $\quad c_3 = (r_{6z} - g_{6z})$

$d_3 = {\ell_6}^2 - {a_3}^2 - {b_3}^2 - {c_3}^2$

By subtracting (3.29) from (3.28) and (3.30) from (3.29) the pesky squared terms can be eliminated, yielding (3.31) and (3.32).

$$2(a_1 - a_2)p_1 + 2(b_1 - b_2)p_2 + 2(c_1 - c_2)p_3 = d_1 - d_2 \quad (3.31)$$

$$2(a_2 - a_3)p_1 + 2(b_2 - b_3)p_2 + 2(c_2 - c_3)p_3 = d_2 - d_3 \quad (3.32)$$

In this step some information is lost in the subtracting out of squared terms. Thus, only two linearly independent equations can be found by subtracting equations, instead of three. This yields an under constrained system of two equations in three unknowns. This loss of information will have to be accounted for later.

Writing (3.31) and (3.32) in matrix form yields:

$$2\begin{bmatrix} a_1 - a_2 & b_1 - b_2 & c_1 - c_2 \\ a_2 - a_3 & b_2 - b_3 & c_2 - c_3 \end{bmatrix}\boldsymbol{p} = \begin{bmatrix} d_1 - d_2 \\ d_2 - d_3 \end{bmatrix} \tag{3.33}$$

Or:

$$M\boldsymbol{p} = \boldsymbol{d} \tag{3.34}$$

Where $M = 2\begin{bmatrix} a_1 - a_2 & b_1 - b_2 & c_1 - c_2 \\ a_2 - a_3 & b_2 - b_3 & c_2 - c_3 \end{bmatrix}$ and $\boldsymbol{d} = \begin{bmatrix} d_1 - d_2 \\ d_2 - d_3 \end{bmatrix}$.

The solution space for this under-constrained system can be described by the sum of the particular and homogeneous solution:

$$\boldsymbol{p} = \boldsymbol{k} + \boldsymbol{h}p_0 \tag{3.35}$$

Where:

$$\boldsymbol{k} = M^{+}\boldsymbol{d}$$

$$\boldsymbol{h} = \mathcal{N}(M)$$

Here $\mathcal{N}(M)$ represents an orthonormal basis for the null space of M, and M^{+} represents the Moore Penrose pseudo-inverse of M.

This represents a one-dimensional solution space with the scalar p_0 as the generalized coordinate of this solution space. The solution to the original system of non-linear equations will lie in this solution space. A single solution does not yet emerge since one

linearly independent equation in the system was lost in the subtraction of equations. To find the solution to the original system, (3.35) can be substituted into (3.19):

$$\|\boldsymbol{k} + \boldsymbol{h}p_0 + \boldsymbol{r}_1 - \boldsymbol{g}_1\| = \ell_1 \tag{3.36}$$

Calculating the vector norm and moving all terms to the left-hand side yields**:**

$$\sqrt{(k_x + h_x p_0 + r_{1x} - g_{1x})^2 + (k_y + h_x p_0 + r_{1y} - g_{1y})^2 + (k_z + h_z p_0 + r_{1z} - g_{1z})^2} - \ell_1 = 0 \tag{3.37}$$

This is now a single non-linear equation that can be solved for p_0 using a numerical method such as Newton-Raphson. This is the method that is used in the Matlab code to generate results used herein. Once p_0 is found, it can be substituted into (3.35) to yield $\boldsymbol{p}$, the position of the end effector.

It is possible for (3.37) to have two real solutions that will lead to two valid end effector positions. These two possible robot poses have to be compared to show which represents the physically realizable configuration. If the cable lengths are such that there is not a physically possible end effector solution, (3.37) will not have a real solution.

Jacobian

To control SkyBAAM it is not only necessary to go from end effector position to cable lengths, but it is also necessary to be able to find cable velocities from end effector velocity. This is done with a Jacobian mapping.

The target end effector velocity is known in the cartesian space, while the cable velocities are required in the joint space. The Jacobian matrix, *J*, defines a linear relation between the cartesian and joint space velocities [27].

$$\dot{\boldsymbol{q}} = J\dot{\boldsymbol{x}} \tag{3.38}$$

Where $\dot{\boldsymbol{q}}$ represents joint, or cable, velocities and $\dot{\boldsymbol{x}}$ represents end effector velocity and angular velocity in Cartesian space. Note that this definition of the Jacobian is backwards from the conventional Jacobian definition for serial robots. For parallel robot finding the traditional Jacobian can often only be done numerically [28]. The Jacobian defined as above for a CDPM with *n* cables is given in the literature [27] as:

$$J = \begin{bmatrix} \hat{\boldsymbol{u}}_1 & \hat{\boldsymbol{u}}_2 & \dots & \hat{\boldsymbol{u}}_n \\ \boldsymbol{r}_1 \times \hat{\boldsymbol{u}}_1 & \boldsymbol{r}_2 \times \hat{\boldsymbol{u}}_2 & \dots & \boldsymbol{r}_n \times \hat{\boldsymbol{u}}_n \end{bmatrix}^T \tag{3.39}$$

Since there are six motion and two tension cables for a total of eight cables, the Jacobian that includes the joint space of all cables is given by (3.40) below. This will be termed the full Jacobian because it maps six DOF end effector velocity to the velocities of all eight joints.

$$J_{full} = \begin{bmatrix} \hat{\boldsymbol{u}}_1 & \hat{\boldsymbol{u}}_2 & \dots & \hat{\boldsymbol{u}}_8 \\ \boldsymbol{r}_1 \times \hat{\boldsymbol{u}}_1 & \boldsymbol{r}_2 \times \hat{\boldsymbol{u}}_2 & \dots & \boldsymbol{r}_8 \times \hat{\boldsymbol{u}}_8 \end{bmatrix}^T \tag{3.40}$$

Here $\dot{\boldsymbol{q}} = \left[\dot{\ell}_1, \dot{\ell}_2, \dot{\ell}_3\ \dot{\ell}_4, \dot{\ell}_5, \dot{\ell}_6, \dot{\ell}_7, \dot{\ell}_8\right]^T$ and $\dot{\boldsymbol{x}} = \left[\dot{x}, \dot{y}, \dot{z}, \dot{\theta}_x, \dot{\theta}_y, \dot{\theta}_z\right]^T$ and J_{full} is a 6x8 matrix that is a mapping between the two.

Because the system was designed to have no rotation of the end effector, $\dot{\theta}_x = \dot{\theta}_y = \dot{\theta}_z = 0$. Since $\dot{\theta}_x = \dot{\theta}_y = \dot{\theta}_z = 0$, and there is the cable length restriction of $\ell_1 = \ell_2 = \ell_3$ and $\ell_4 = \ell_5$, and cables 7 and 8 do not contribute to the motion of the system, it is also valuable to have a matrix that maps cartesian velocity only, to the velocity of cables 1, 4, and 6 only. This will be called the 3D Jacobian since it maps three DOF velocity to the velocity of three defining joints. To find these a subset of the full Jacobian can be taken. This subset is the entries that are on rows 1, 4 and 6 and on columns 1, 2 and 3. Thus:

$$J_{3D} = J_{full_{[1,4,6],[1,2,3]}} = [\hat{\boldsymbol{u}}_1 \quad \hat{\boldsymbol{u}}_4 \quad \hat{\boldsymbol{u}}_6]^T \tag{3.41}$$

With:

$$\dot{\boldsymbol{q}}' = J_{3D}\dot{\boldsymbol{x}}' \tag{3.42}$$

Where the cable velocity vector and the end effector velocity vector are represented by $\dot{\boldsymbol{q}}' = \left[\dot{\ell}_1, \dot{\ell}_4, \dot{\ell}_6\right]^T$ and $\dot{\boldsymbol{x}}' = [\dot{x}, \dot{y}, \dot{z}]^T$ respectively.

Both of these Jacobians will be used in later analysis.

Cable Tension

The above defines the motion cables. It does not take into account the tensions cables and how they affect the system. As was seen above, it is important to maintain a minimum tension on the cables. In the SkyBAAM system there are two tensioning cables. By changing the tension in these two cables the net tension vector on the system can be controlled to a degree. In this section a method for determining the tension in these cables will be derived.

In the literature [27] the static balance of the end effector of a CDPM has been found as:

$$J_{full}{}^T \boldsymbol{\tau} = -\boldsymbol{F_e} \tag{3.43}$$

Here $\boldsymbol{\tau}$ is a vector of cable tensions and $\boldsymbol{F_e}$ is a vector of external forces and moments on the end effector, including gravity. Using D'Alembert's principle, inertial forces on the end effector due to motion can be included in $\boldsymbol{F_e}$.

Because this is a six DOF system with eight cables, (3.43) is an under-constrained system. Equation (3.43) is a system of six equations with eight unknowns. Thus, there are in general an infinite number of solutions to the static balance equation. There are two redundant degrees of freedom in this system of equations. By setting two of the tensions, the system will become exactly constrained and a single solution will emerge for the tension in all the cables. In SkyBAAM, the tension of both the *x'* and *y'* cables is actively controlled, providing the needed reduction in degrees of freedom. By changing the tension set points on the *x'* and *y'* cables the solution space of (3.43) can be explored. The challenge is to find the optimum location in that solution space to determine the tension set points for *x'* and *y'*.

The full set of possible cable tensions is found by sum of the particular and homogeneous solutions of (3.43) [29].

$$\boldsymbol{\tau} = \boldsymbol{k} + H\boldsymbol{\tau}_0 \tag{3.44}$$

Where the particular and homogeneous solutions are found by:

$$\boldsymbol{k} = ({J_{full}}^T)^+(-\boldsymbol{F_e}) \tag{3.45}$$

$$H = \mathcal{N}({J_{full}}^T) \tag{3.46}$$

The vector of cable tensions, $\boldsymbol{\tau}$, is an 8x1 vector. The solution space is parametrized with vector $\boldsymbol{\tau}_0$ which is any real 2x1 vector. The length of $\boldsymbol{\tau}_0$ being two is a result of the two redundant degrees of freedom.

The particular solution physically represents tension in the cables dues to $\boldsymbol{F_e}$. The homogeneous solution represents tensions internal to the system that arise from the redundant degrees of freedom. Physically this is tension caused by the *x'* and *y'* tension cables. It will be noted that the homogenous solution does not affect the net forces or moments on the system. Mathematically this is shown in (3.47) which is a substitution of the homogenous solution into (3.43) and taking advantage of the properties of the null space.

$${J_{full}}^T H\boldsymbol{\tau}_0 = 0 \tag{3.47}$$

It is now necessary to find $\boldsymbol{\tau}_0$ which will yield the optimum tension values. Earlier in the chapter the asymptotic nature of cable stiffness with respect to cable tension was discussed. It is desirable to keep cable stiffnesses high to improve system performance. Thus, the first optimization goal will be to keep all cables at or above a minimum tension that keeps the stiffness within a certain window of the asymptotic stiffness. For the SkyBAAM system developed at ORNL all motion cable stiffnesses are kept at or above 95% of the asymptotic stiffness. The minimum tensions to achieve this will be designated as $\boldsymbol{\tau}_{min}$. For cable *i*:

$$k_{net_i}|_{t=\tau_{min_i}} = .95 * \lim_{t\to\infty} k_{net_i} \tag{3.48}$$

Substituting in (3.16) and (3.17) this becomes:

$$\frac{300D^2(\ell^2 w^2 \tau_{min_i} + 8{\tau_{min_i}}^3)}{24G\ell{\tau_{min_i}}^3 + \ell^3 w^2(200D^2\ell + 3G\tau_{min_i})} = 95\frac{D^2}{G\ell} \tag{3.49}$$

Rearranging:

$$f(\tau_{min_i}) = \frac{300D^2(\ell^2 w^2 \tau_{min_i} + 8{\tau_{min_i}}^3)}{24G\ell{\tau_{min_i}}^3 + \ell^3 w^2(200D^2\ell + 3G\tau_{min_i})} - 95\frac{D^2}{G\ell} = 0 \tag{3.50}$$

Close form analytical solutions for τ_{min_i} are not tractable, so this must be solved numerically. As discussed in the section on composite stiffness above, and illustrated in Figure 3.4, the stiffness of a cable increases monotonically from zero to the asymptotic value. Because of the monotonic nature of cable stiffness, the Newton Raphson method can be used to solve for τ_{min_i} in (3.50). Exhaustive search methods could also be used.

Numerically solving (3.50), the entries of $\boldsymbol{\tau}_{min}$ can be populated for cables 1 through 5. Cable 6 is primarily in the vertical direction so catenary sag is not an issue. Therefore, it only has the requirement that it not be in compression so, $\tau_{min_6} = 0$. Catenary sag is not an issue for the tension cables either, since they are not used for position control, so they also have a minimum tension of 0, or $\tau_{min_7} = \tau_{min_8} = 0$.

Now the following constrain can be put on the optimization:

$$\boldsymbol{\tau} \geq \boldsymbol{\tau}_{min} \tag{3.51}$$

An objective function to minimize for the optimization is also needed. It is desirable to reduce unnecessary tension in the system [30]. This leads to lower energy consumption, smaller servos, and smaller mechanical components required for the system. In order to get a measure of the total tension the system is under, the Euclidian norm of the vector $\boldsymbol{\tau}$ of all the tensions can be taken. Using the norm to minimize tension is consistent with the work of Gosselin and Grenier [31]. The objective function to minimize is thus:

$$f(\boldsymbol{\tau}) = \|\boldsymbol{\tau}\| \tag{3.52}$$

The optimization can now be written as:

$$\min\{\|\boldsymbol{\tau}\| \,|\boldsymbol{\tau} \geq \boldsymbol{\tau}_{min}\} \tag{3.53}$$

To determine the solution space that satisfies the constraint, (3.44) is substituted into (3.51) yielding:

$$\boldsymbol{k} + H\boldsymbol{\tau}_0 \geq \boldsymbol{\tau}_{min} \tag{3.54}$$

This is a system of eight inequalities with two unknowns contained in the vector $\boldsymbol{\tau}_0$. Oh and Agrawal [24], recognized that this system of inequalities defines a convex polytope forming what they termed a feasible space. Their method will be followed here.

Each equation in (3.55) defines a line in the two-dimensional space of $\boldsymbol{\tau}_0$ with the space on one side of this line satisfying the inequality. If the solution space of (3.54) is not the null set, then the eight inequalities will bound an area for $\boldsymbol{\tau}_0$ which satisfies (3.54) called the feasible space.

This is graphically shown in Figure 3.6. This figure shows a hypothetical case of eight linear inequalities as given in (3.54). The lines defining the boundaries of each linear inequality are plotted. The *x* and *y* axes are the two elements of the vector parameter $\boldsymbol{\tau}_0$. The area satisfying all the linear inequalities is shown in grey. This is the area for $\boldsymbol{\tau}_0$ that satisfies (3.51), and is what was termed by Oh and Agrawal the feasible space. Any $\boldsymbol{\tau}_0$ value in the feasible space can be substituted into (3.44) to yield a tension that satisfies the constraint of (3.51)

Oh and Agrawal demonstrated that the optimum locations are at the corners of this space. The corners of this space are found by the intersection of the lines. First, every possible intersection of lines is found. Writing (3.55) as an equality instead of an inequality yields:

$$\boldsymbol{\tau}_{min} = \boldsymbol{k} + H\boldsymbol{\tau}_0 \tag{3.55}$$

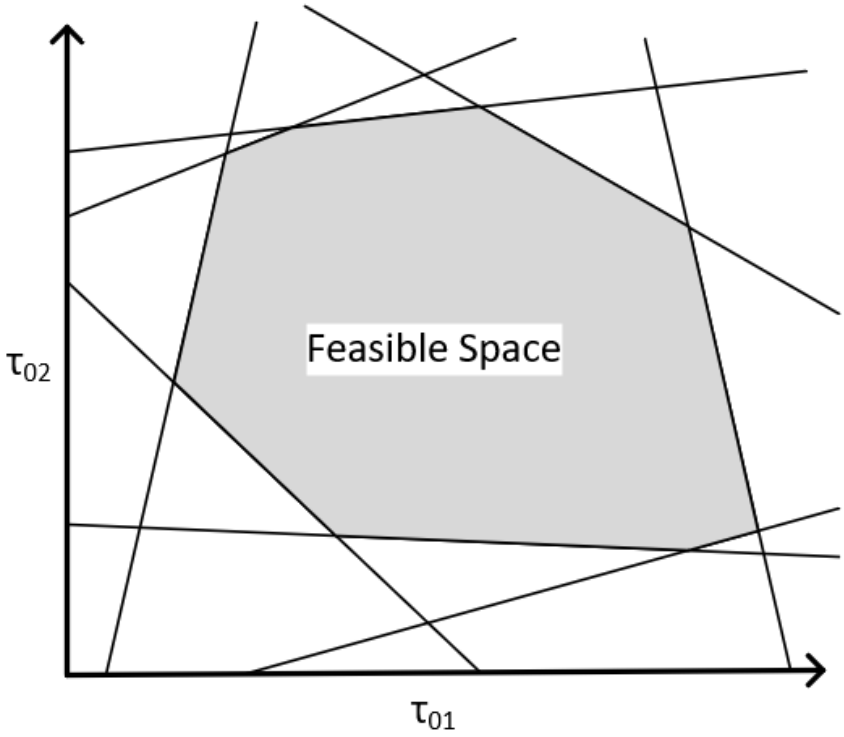

Figure 3.6 Feasible Space for Tension

Rearranging:

$$\boldsymbol{\tau}_{min} - \boldsymbol{k} = H\boldsymbol{\tau}_0 \tag{3.56}$$

Or:

$$\boldsymbol{s} = H\boldsymbol{\tau}_0 \tag{3.57}$$

Where

$$\boldsymbol{s} = \boldsymbol{\tau}_{min} - \boldsymbol{k} \tag{3.58}$$

This a system of eight equations with two unknowns equivalent to (3.54). Every intersection of these equations can be found by:

$$\boldsymbol{\tau_0}^*_{\boldsymbol{k}} = \begin{bmatrix} H_{i,*} \\ H_{j,*} \end{bmatrix}^{-1} \begin{bmatrix} s_i \\ s_j \end{bmatrix} \tag{3.59}$$

Where $H_{i,*}$ is the i^{th} row of H, and $1 \leq i \leq 7$, and $(i+1) \leq j \leq 8$. This gives 56 intersection points, $\boldsymbol{\tau_0}^*_{\boldsymbol{k}}$, for $k = 1$ to $k = 56$. Substituting each $\boldsymbol{\tau_0}^*_{\boldsymbol{k}}$ into (3.44) gives 56 potential values for $\boldsymbol{\tau}$. This set of potential values for $\boldsymbol{\tau}$ is reduced to those that satisfy the constraint equation (3.51). These are the points on the corners of the feasible space.

The final value for $\boldsymbol{\tau}$ is then found from the set of corner points by finding the one which gives the lowest value for the objective function (3.52). The tension values for cables 7 and 8 will be set points for the tension control loops on the tension cables, *x'* and *y'*. These values will change as the end effector moves through the workspace.

Stiffness Matrix

In the literature a method for determining the stiffness matrix has been found [27]. This will be used later to calculate performance indices. This method is summarized below.

The stiffness matrix, K, of the end effector is given by:

$$K = K_s + K_f \tag{3.60}$$

Where

$$K_s = \sum_{i=1}^{n}\left(k_i - \frac{\tau_i}{\ell_i}\right)\begin{bmatrix} \hat{\boldsymbol{u}}_i\hat{\boldsymbol{u}}_i^T & \hat{\boldsymbol{u}}_i\hat{\boldsymbol{u}}_i^T[\boldsymbol{r}_i\times]^T \\ [\boldsymbol{r}_i\times]\hat{\boldsymbol{u}}_i\hat{\boldsymbol{u}}_i^T & [\boldsymbol{r}_i\times]\hat{\boldsymbol{u}}_i\hat{\boldsymbol{u}}_i^T[\boldsymbol{r}_i\times]^T \end{bmatrix} + \sum_{i=1}^{n}\frac{\tau_i}{\ell_i}\begin{bmatrix} I_{3x3} & [\boldsymbol{r}_i\times]^T \\ [\boldsymbol{r}_i\times] & [\boldsymbol{r}_i\times][\boldsymbol{r}_i\times]^T \end{bmatrix} \tag{3.61}$$

And

$$K_f = \sum_{i=1}^{n}\tau_i\begin{bmatrix} \mathbf{0}_{3x3} & \mathbf{0}_{3x3} \\ \mathbf{0}_{3x3} & [\hat{\boldsymbol{u}}_i\times][\boldsymbol{r}_i\times] \end{bmatrix} \tag{3.62}$$

Here $[\boldsymbol{r}_i\times]$ represents the cross-product operator, or skew matrix defined as:

$$[\boldsymbol{r}_i\times] = \begin{bmatrix} 0 & -r_z & r_y \\ r_z & 0 & -r_x \\ -r_y & r_x & 0 \end{bmatrix} \tag{3.63}$$

For $\boldsymbol{r}_i = [r_x, r_y, r_z]^T$.

In (3.61) and (3.62) $\hat{\boldsymbol{u}}_i$ is the unit vector along cable *i* as defined previously. The tension in cable *i* is τ_i as found previously. The vector $\boldsymbol{r}_i$ is as defined previously. The length of cable *i*, found from the inverse kinematics is ℓ_i. The stiffness of cable *i* is k_i found from (3.16).

In the following chapter the stiffness matrix will be used to calculate a stiffness index that will be used the characterize performance throughout the workspace.

Summary

This chapter developed a mathematical model for the SkyBAAM cable configuration. This included the forward and inverse kinematics and Jacobian. A model of how cable tension effects stiffness was also developed along with a way of controlling cable tension in the system. Finally, a method for calculating the stiffness of the end effector was shown. These

models will be used in the next chapter to analyze and understand the performance of the whole system.

Chapter Four
SYSTEM ANALYSIS

The models for the SkyBAAM system developed in the previous chapter will be used presently to analyze the performance of the system as the end effector traverses the workspace, and also to bound the workspace. A stiffness index is developed to understand how the end effector stiffness changes throughout the workspace. Then singularities are found and the workspace is defined.

After these are defined, the system designed at ORNL will be examined and the performance will be plotted over the workspace. Finally, a comparison of cable types will be made to understand scaling to larger sizes on future systems.

Stiffness Index

CDPRs are inherently relatively low stiffness manipulators. Furthermore, the stiffness will change throughout the workspace as cable lengths change. It is important to be able to quantify what the actual system stiffness is to understand how the system will perform and what tasks it can accomplish.

The previous chapter gives the full 6x6 stiffness matrix of the end effector derived in literature. However, it would be useful to know how the tip defects in the *x-y* plane due to inertial forces at the center of mass. This will help convert the full stiffness matrix into an easily usable metric. This information needs to be extracted from the full 6x6 matrix. In keeping with the rest of this work, it is determined that the stiffness matrix is derived with the origin at the deposition tip.

The stiffness matrix relates force and displacement as follows:

$$\boldsymbol{F_e} = K\boldsymbol{\Delta} \tag{4.1}$$

Where $\boldsymbol{F_e}$ is the vector force on the end effector and $\boldsymbol{\Delta}$ is the vector displacement of the end effector. From the stiffness matrix, the compliance matrix is defined as:

$$C = K^{-1} \tag{4.2}$$

This allows displacements to be found from known forces:

$$\boldsymbol{\Delta} = C\boldsymbol{F_e} \tag{4.3}$$

This yields a 6x1 displacement vector including both translation and rotation from a 6x1 force vector including both forces and moments. However, for this system a maximum *x*-*y* plane displacement resulting from an *x*-*y* plane force is a useful measurement since the system operates with primarily *x*-*y* motion. The location of this force will be taken at the center of mass since the primary forces on the end effector will be inertial.

For an *x*-*y* force $\boldsymbol{f}$, the deflection in the *x*-*y* plane from the force is:

$$\boldsymbol{\Delta}_1 = \begin{bmatrix} C_{1,1} & C_{1,2} \\ C_{2,1} & C_{2,2} \end{bmatrix} \boldsymbol{f} \tag{4.4}$$

If the force acts at the center of mass, there is also a deflection due to the moment about the tip. Let $\boldsymbol{\ell}_{cm}$ represent a vector from end effector origin to center of mass. The end effector for SkyBAAM is largely symmetrical about the *x*-*z* place and the *y*-*z* plane. Thus, we can assume the center of mass to be over the end effector origin which implies the only non-zero element of the vector $\boldsymbol{\ell}_{cm}$ is in the *z* direction.

The moment of the *x*-*y* components of the force about the origin is:

$$\boldsymbol{m} = \begin{bmatrix} f_1 \\ f_2 \\ 0 \end{bmatrix} \times \boldsymbol{\ell}_{cm} \tag{4.5}$$

With the assumption from above that only the *z* element of $\boldsymbol{\ell}_{cm}$ is non-zero this yields:

$$\boldsymbol{m} = \ell_{cm\ 3} \begin{bmatrix} f_1 \\ f_2 \\ 0 \end{bmatrix} \tag{4.6}$$

Or ignoring the zero *z*-component of the moment:

$$\boldsymbol{m}' = \ell_{cm\ 3} \begin{bmatrix} f_1 \\ f_1 \end{bmatrix} \tag{4.7}$$

Taking the components of the compliance matrix that cause an *x* or *y* displacement from these moments yields the following:

$$\boldsymbol{\Delta}_2 = \begin{bmatrix} -C_{1,4} & C_{1,5} \\ -C_{2,4} & C_{2,5} \end{bmatrix} \ell_{cm\ 3} \begin{bmatrix} f_1 \\ f_1 \end{bmatrix} \tag{4.8}$$

The force components can be rearranged to yield:

$$\boldsymbol{\Delta}_2 = \ell_{cm\ 3} \begin{bmatrix} -C_{1,5} & C_{1,4} \\ -C_{2,5} & C_{2,4} \end{bmatrix} \boldsymbol{f} \tag{4.9}$$

The total deflection is the sum of these two types of deflection of the deposition tip:

$$\boldsymbol{\Delta} = \boldsymbol{\Delta}_1 + \boldsymbol{\Delta}_2 = C'\boldsymbol{f} \tag{4.10}$$

Where:

$$C' = \begin{bmatrix} C_{1,1} & C_{1,2} \\ C_{2,1} & C_{2,2} \end{bmatrix} + \ell_{cm\ 3} \begin{bmatrix} -C_{1,5} & C_{1,4} \\ -C_{2,5} & C_{2,4} \end{bmatrix} \tag{4.11}$$

C' represents a mapping from an *x*-*y* force at the center of mass to an *x*-*y* displacement at the end effector origin which is coincident with the point of deposition. If the force applied is a unit magnitude, the total possible forces from any direction represent a circle. C' maps this circle in force space to an ellipse in displacement space. This is graphically shown in Figure 4.1.

The eigenvectors of C' represent the major and minor axes of the ellipse and the eigenvalues represent the magnitude of the axes. The maximum deflection for a given force of magnitude, $\boldsymbol{f}$, will occur when $\boldsymbol{f}$ is directed along the major axis. Using the largest eigenvalue, this deflection will have a magnitude of:

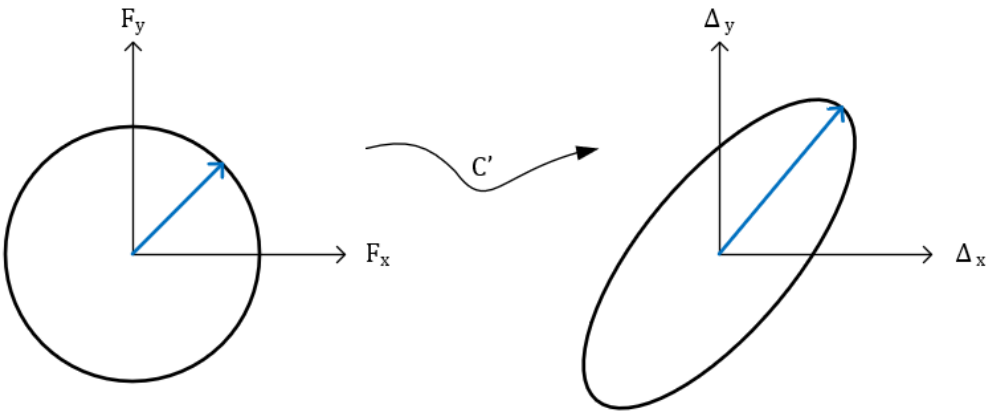

Figure 4.1 Force to Displacement Mapping

$$\delta = \lambda_1 F \tag{4.12}$$

Thus, a useful stiffness index is λ_1, the largest eigenvalue of C'. λ_1 has units of $\frac{inches}{lbf}$ and represents the maximum displacement possible at the end effector per pound force applied at the center of mass. The values for λ_1 across the workspace for the ORNL system will be plotted later in the chapter.

Singularities

The previously defined 3D Jacobian is:

$$J_{3D} = [\hat{\boldsymbol{u}}_1 \quad \hat{\boldsymbol{u}}_4 \quad \hat{\boldsymbol{u}}_6]^T \tag{4.13}$$

This represents the following mapping:

$$\dot{\boldsymbol{q}}' = J_{3D}\dot{\boldsymbol{x}}' \tag{4.14}$$

Where $\dot{\boldsymbol{q}}' = \left[\dot{\ell}_1, \dot{\ell}_4, \dot{\ell}_6\right]^T$ and $\dot{\boldsymbol{x}}' = [\dot{x}, \dot{y}, \dot{z}]^T$.

The three-dimensional singularities of the end effector will occur where J_{3D} loses full rank, or in other words its determinate equals zero. This happens when two rows or columns are equal. It is apparent that this happens when $\hat{\boldsymbol{u}}_1 = \hat{\boldsymbol{u}}_4$ or $\hat{\boldsymbol{u}}_1 = \hat{\boldsymbol{u}}_6$ or $\hat{\boldsymbol{u}}_4 = \hat{\boldsymbol{u}}_6$. This means that the system is at a singularity when the *x* and *y*-cables are parallel, the *x* and *z*-cables are parallel, or the *y* and *z*-cables are parallel.

Workspace

The groundwork needed to derive the workspace of the system has now been laid. The workspace will be developed using the concepts in the sections above on singularities and tension.

At a minimum, the tensions of the cables must be above the minimum tensions defined previously. However, at some points the required tension is not attainable. As these points in the workspace are approached, the overall tension distribution in the system cannot be

managed readily. In other words, some cables will end up seeing very high tensions to keep others at their minimum tension. This tension distribution will be quantified through the use of a tension margin index, η.

The minimum required tensions for the system, that have previously been found, are given in the vector $\boldsymbol{\tau}_{min}$. The 2-norm of this vector, $\|\boldsymbol{\tau}_{min}\|$, gives a measurement of the "size" of this vector, or the total tension that the system is under at this minimum tension point. However, this minimum tension point is only theoretical and the actual tensions, $\boldsymbol{\tau}$, are found as described above and will generally be higher than $\boldsymbol{\tau}_{min}$. The 2-norm of $\boldsymbol{\tau}$ can be used as a measure of the how much tension the system is actually under. By taking a ratio of these two values a measure is obtained of how much higher the actual system tension is than the required system tension. This will be defined as the tension margin value (4.15).

$$\eta = \frac{\|\boldsymbol{\tau}_{min}\|}{\|\boldsymbol{\tau}\|} \tag{4.15}$$

This value is bounded from 0 to 1 exclusive of 0. When this value is 1, the actual tension is the same as the minimum tension. However, in general $\|\boldsymbol{\tau}\|$ will be higher than $\|\boldsymbol{\tau}_{min}\|$ since some of the cables will be above the minimum tensions while others are at the minimum tension. If some or all of the cables have very high tensions, η will approach zero.

Setting a minimum threshold for η limits these areas where some cables have very high tensions. If η for a given point is below this threshold then that point is considered outside of the workspace. This threshold can be chosen in a way that makes sense when building a specific embodiment of the SkyBAAM system. A higher threshold will lead to a smaller workspace, but lower tensions that the system must achieve, while a lower threshold will increase the workspace, but will also increase the required tension the system must be able to handle. In the development of the ORNL system, 0.2 was chosen as the threshold value.

Secondly singularities must be avoided in the workspace of the system. As discussed above this happens when the determinate of J_{3D} becomes equal to zero. As the system approaches

singularities, the manipulability of the system decreases. Thus, to avoid getting close to the singularities and their reduction in manipulability a minimum threshold for determinate of J_{3D} can be chosen. For the system built at ORNL a minimum threshold of 0.5 was chosen.

The threshold values that were chosen for η and the determinate of the Jacobian were based on engineering judgment for a balance between workspace size, tension available from the servo motors, and system performance. This is discussed in more detail in the section on analysis of the ORNL SkyBAAM System.

In summary the workspace of the system is defined as all the points that satisfy the following requirements:

$$\eta > 0.2$$

$$\det(J_{3D}) > 0.5$$

As previously mentioned, the values given for the thresholds are based on engineering judgment and effect the system requirements and workspace size.

Analysis of the ORNL SkyBAAM System

The system designed at ORNL nominally has the layout and dimensions shown in Figure 4.2. Further discussion of the fabricated system is given in chapter five, the goal of this section being to evaluate the system using the theoretical methods previously derived.

The position of the cable winders was measured with a Leica AT960 laser tracker. These positions are summarized in Table 4.1 and the geometry of the end effector is summarized in Table 4.2. Units in these tables are in inches. This system uses 1/8” 7x19 steel wire rope for cables with a weight of .0024 lbs/in. The *G* value for calculating cable stiffness for this cable is 0.000014 [26].

Using this system configuration information, the ORNL system is analyzed using the techniques developed previously in chapters two and three and the results plotted. The MATALB code for this is found in the Appendix.

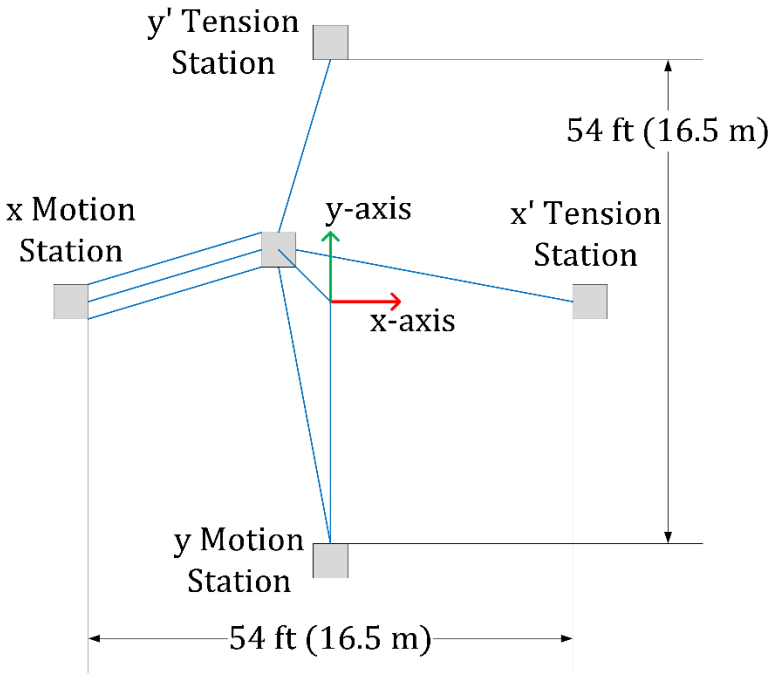

Top View

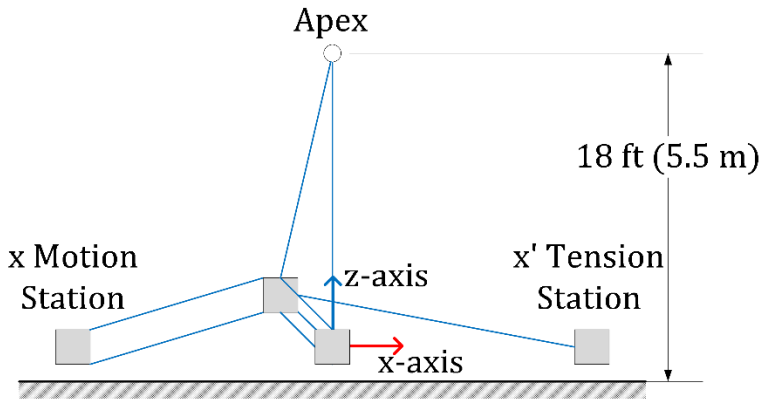

Side View

Figure 4.2 ORNL SkyBAAM Layout

Table 4.1 Base Station Configuration

X Motion			Y Motion		Z Motion	X' Tension	Y' Tension
$\boldsymbol{g}_1$	$\boldsymbol{g}_2$	$\boldsymbol{g}_3$	$\boldsymbol{g}_4$	$\boldsymbol{g}_5$	$\boldsymbol{g}_6$	$\boldsymbol{g}_7$	$\boldsymbol{g}_8$
328.94	328.94	328.94	36.24	36.24	0	-348.19	4.88
-33.82	-45.82	-21.82	329.05	392.05	0	-20.43	-347.0
36.78	0.78	.78	37.26	1.26	201.66	35.12	35.25

Table 4.2 End Effector Configuration

X Motion			Y Motion		Z Motion	X' Tension	Y' Tension
$\boldsymbol{r}_1$	$\boldsymbol{r}_2$	$\boldsymbol{r}_3$	$\boldsymbol{r}_4$	$\boldsymbol{r}_5$	$\boldsymbol{r}_6$	$\boldsymbol{r}_7$	$\boldsymbol{r}_8$
12	12	12	0	0	0	-12	0
0	-12	-12	12	12	0	-0	-12
52	16	16	52	16	34	34	34

First the workspace is found. This is done by numerically searching for points that satisfy the workspace constraints. This is plotted in Figure 4.3. The locations of the cable winders are shown in red and the cables are shown for the end effector at the center of the workspace.

It can be seen that the workspace gets narrower in the *x-y* plane closer to the top of the workspace, while being much wider near the bottom. A large portion of the workspace is below the cable winding points. This workspace is somewhat limiting for building practical structures, as most buildings maintain the same footprint for most of their height. There is, however, a way to get around these limitations. By mechanically moving the cable winders up on some sort of rail, the workspace could be moved up incrementally and the widest parts of the workspace utilized throughout the build. This also makes it possible to use the widest part of the workspace at the bottom, that otherwise are below the ground plane and thus inaccessible. However, the cost to gain this improvement is the added mechanical complexity of making the cable winders able move vertically on linear actuators, and the necessity to recalibrate after moving the cable winders.

Looking at the top down view of the workspace, further limitations are evident, with the footprint of the workspace being only a portion of the area between the cable winders, and its shape being irregular. Unless one wants to print buildings in the shape of a four-sided star, this shape is limiting. To fit most prismatic buildings in a shape like this, the system would have to be made quite large. This creates problems, since one must have the necessary space around the building site to fit a large SkyBAAM system. If there are nearby buildings, this may become impossible. A possible way to get around this would be to add more base stations, with only some actively controlling motion at any one time. This way, when singularities are approached, the system could automatically switch to using a different set of cables that would avoid the singularities, increasing the size of the workspace. The same could be done when approaching areas where the required tensions also could not be met. Again, there is an added cost of adding more base stations, and increasing controller complexity.

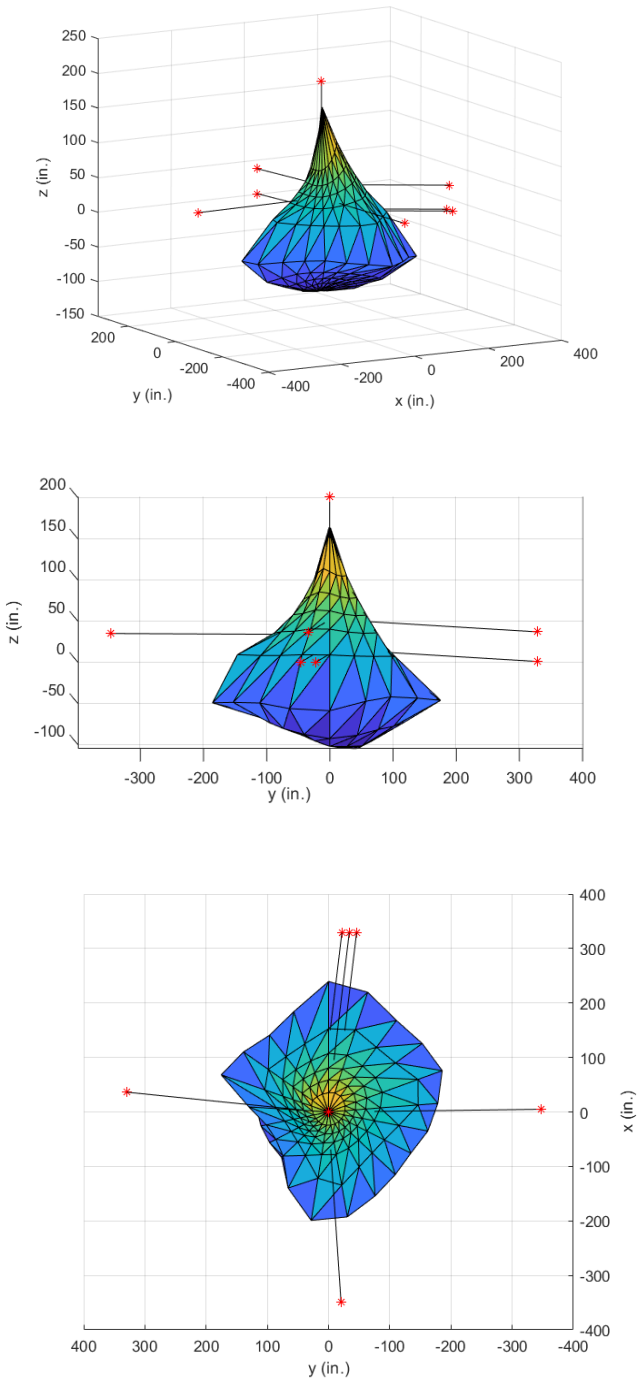

Figure 4.3 Workspace Boundary

With the ORNL SkyBAAM system as it stands, it is obvious that the workspace imposes unfortunate limitations on what types of parts can be built. However, the proposed methods of allowing the base winders to mover vertically and adding more base stations could increase the workspace size and make it more practical. If the SkyBAAM system is to become a viable system for printing buildings commercially, these avenues will likely have to be investigated, and there should be future research in these areas.

To explore how the system performs within the workspace, the stiffness index, λ_1, is also explored. The value for λ_1, is plotted at a number of layers in the workspace in Figure 4.4. To help visualize the distribution of compliance in the workspace, a histogram of λ_1 throughout the workspace is shown in Figure 4.5. Most values are lower than $0.04\,\frac{inches}{lbf}$ while only at the very bottom are higher values seen. This corresponds to an *x*-*y* plane stiffness over most of the workspace being better that $25\,\frac{lbf}{inch}$ with a significant portion better than $50\,\frac{lbf}{inch}$.

Finally, the tension in the various cable winders is plotted throughout the works space. This is shown in Figure 4.6. Here tension in individual cables is not plotted, but the total tension from each cable wider. Thus, the *x* tension value is the sum of the *x*-cables (cables 1-3). The *x'* and *y'* tensions are the tensions that must be supplied by the respective tension cables. The values in these plots were used to design the mechanical components of the system and size the servo drives. A summary of maximum and median tension from these plots is given in Table 4.3.

When designing a system with the SkyBAAM cable configuration, tradeoffs studies can be done by changing the threshold values for the workspace criteria. Doing this will change workspace size and the required tension values needed to achieve that workspace. Slightly larger workspaces can be achieved, but at the cost of higher tension, while lowering the maximum tension will shrink the workspace. It was through doing this that the threshold values given earlier in the chapter were arrived at. However, depending on the exact needs of a system being developed, these can be tweaked.

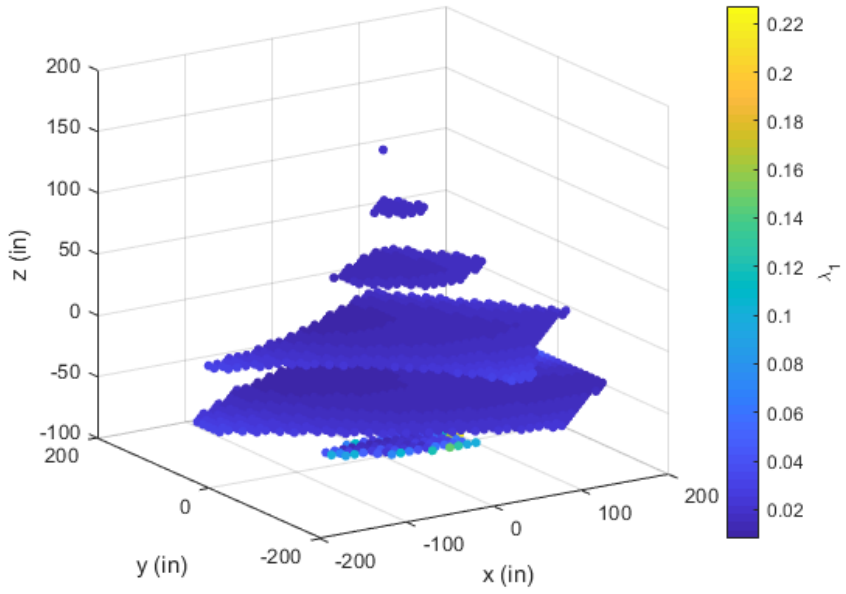

Figure 4.4 Stiffness Index

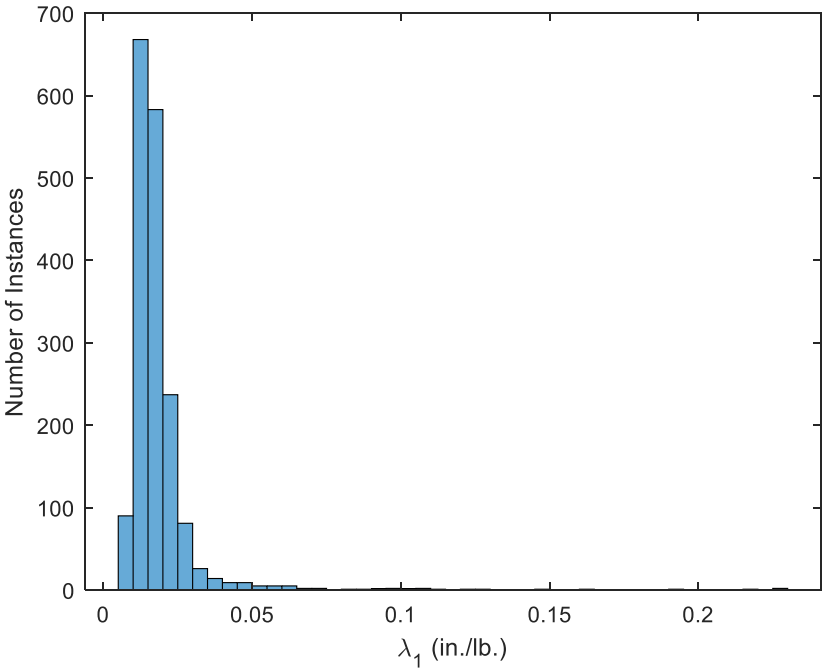

Figure 4.5 Stiffness Distribution

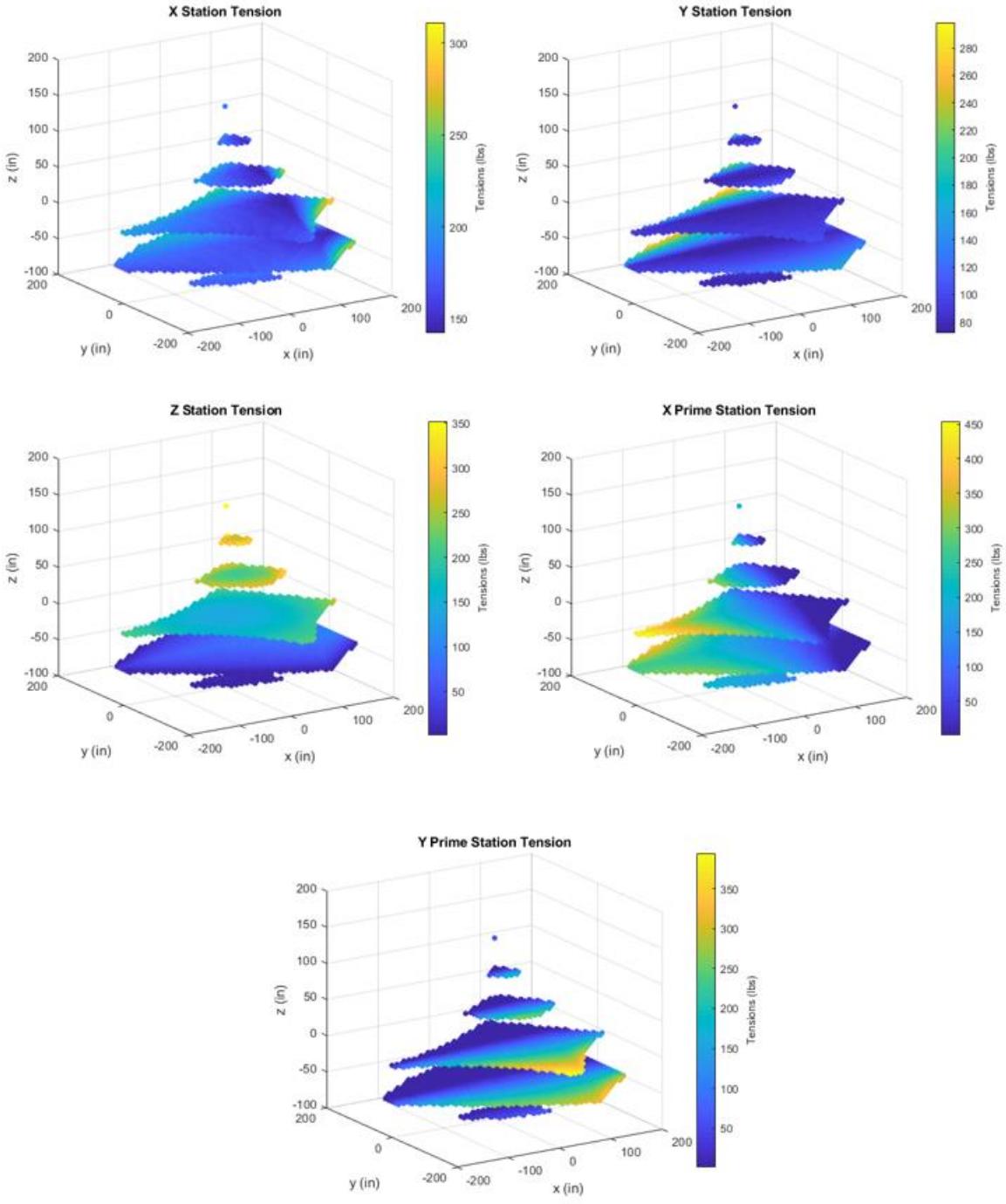

Figure 4.6 Cable Tensions

Table 4.3 Station Tension

Station	**Maximum Tension (lbf)**	**Median Tension (lbf)**
x	311	174
y	299	91
z	352	82
x'	454	159
y'	394	59

Scaling

The SkyBAAM system built at ORNL is meant to be a prototype system that is smaller than eventual systems needed to produce buildings and other large articles, with this smaller system paving the way for larger systems. In order to look towards future use of these systems, the scaling laws in play must be understood. To investigate how this type of system scales, the required tension and required diameter of a single cable in the system will be investigated.

In the previous chapter the method to find the tension dependent stiffness of a cable was derived. Using those results, the stiffness of 7x19 cables of multiple diameters at multiple lengths is plotted in Figure 4.7. From these plots there are several things that can be observed. Consistent with what has already been discussed, for a given length and diameter the stiffness increases with tension until it reaches an asymptote. It can also be seen that the asymptotic stiffness, for a given diameter, decreases for longer cable spans. Furthermore, higher asymptotic stiffness can be achieved by using larger diameters. However, this comes at a cost, namely an increase in required tension. This physically makes sense because the elastic stiffness will go up with the diameter, but the weight also goes up, leading to a requirement of higher tension to overcome the catenary sag.

Another interesting feature emerges when viewing the information in these plots. For a given cable length, there is an optimal cable diameter that gives the highest stiffness at a given tension. As tension increases, the optimal diameter goes up. In other words, higher tension allows for the catenary sag of a larger diameter cable to be overcome.

Armed with the information that at a given length and tension combination, there is an optimal cable diameter, a more complete picture can be painted showing the interplay between cable diameter, length, and tension. A densely populated grid of length and tension combinations is taken. At each of these points the optimal cable diameter can be found, and the stiffness of this cable evaluated. This information is plotted in Figure 4.8 where, for every length and tension combination, the optimal cable diameter and the stiffness are

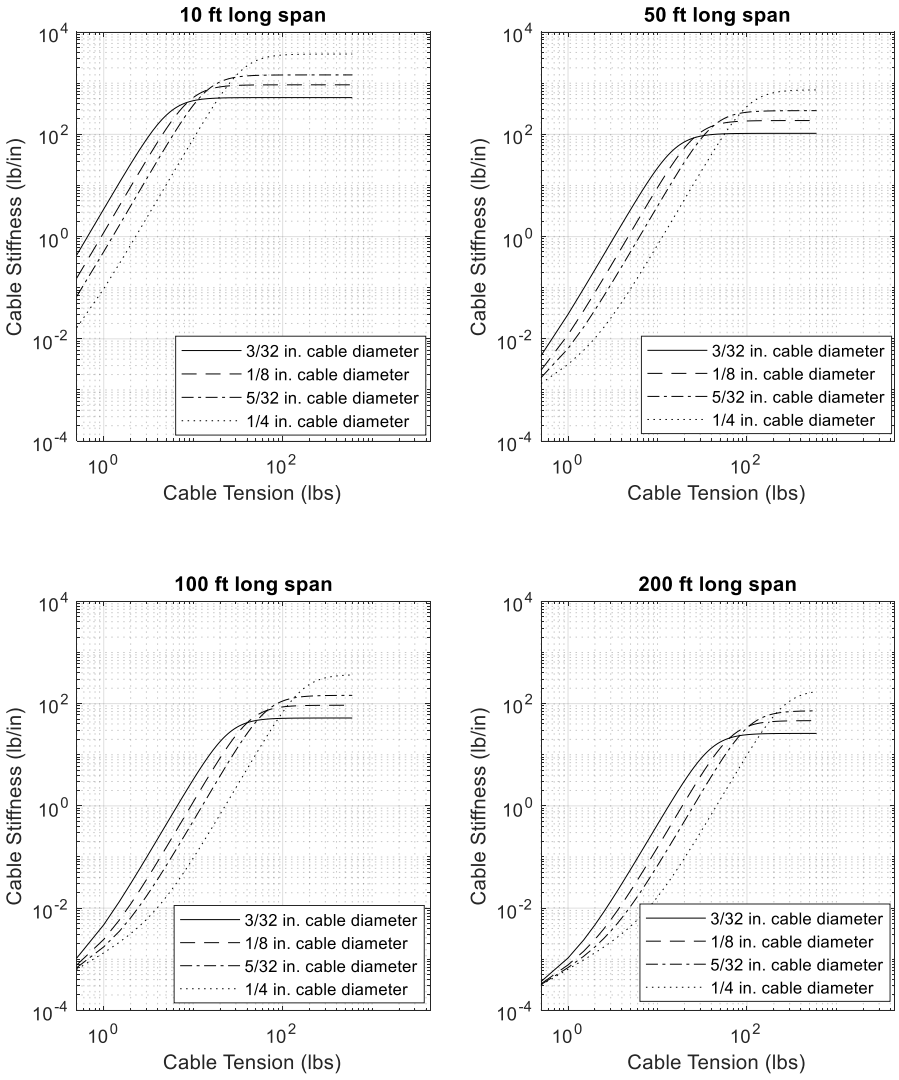

Figure 4.7 Tension and Stiffness for Different 7x19 Cables

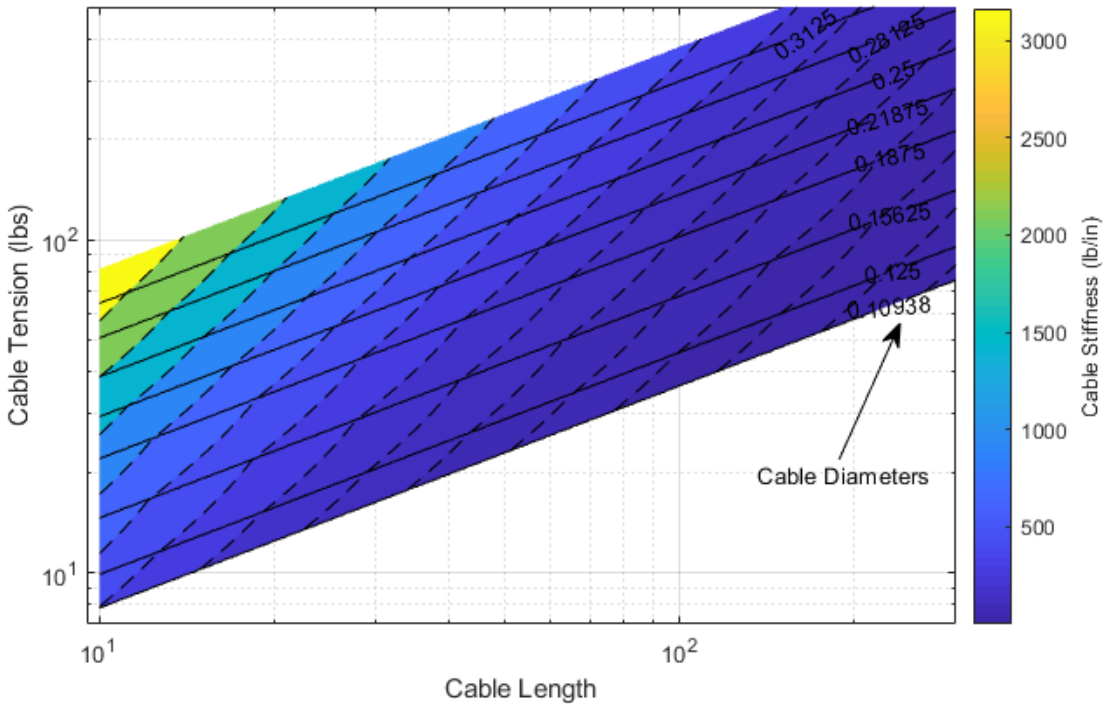

Figure 4.8 7x19 Cable Scaling

plotted together. This figure shows the cable stiffness with color and contours are used to show the regions for each cable diameter.

This figure can be used in designing a system to select the optimal cable diameter, but additionally it gives insight into how SkyBAAM scales. There are several interesting things that can be seen from this plot. At a given length, as tension is increased, the stiffness goes up. However, the cable diameter must also be increased, which is apparent by the cable diameter contours being crossed while moving up in tension. Conversely, at a fixed tension, if the length increases, stiffness and cable diameter drop.

A further observation is made when looking at how a system scales along a constant stiffness contour. If a system has short cables and it is desirous to scale to a larger system with the same performance, a constant stiffness contour line is followed and this will constrain how the tension needs to increase, as well as the required cable diameters. It is noted that these constant stiffness contours in Figure 4.8 are straight lines on a log-log scale, meaning they are power law functions of the form $\tau = A\ell^n$, where τ and ℓ represent tension and length and *A* and *n* are constants that are unique to each contour. Doing a least square fit for multiple contours, *A* and *n* can be found for different stiffnesses. This is tabulated in Table 4.4 where it is seen that the values for *A* vary with stiffness while the values for the exponent, *n*, are roughly constant. The average exponent value is 1.65.

The scaling of a single cable can be taken as a simplified analog for the scaling of the whole system. As a system is scaled up while maintaining equivalent stiffness of the cables, the stiffness of the end effector itself, being a linear combination of the cable stiffnesses, will remain roughly equivalent. With this correlation between the stiffness of individual cables and the end effector stiffness, it is clear that keeping stiffness constant when scaling up the size of a system will scale up tension by a power of 1.65.

The power law nature of scaling in the system creates problems for scaling up to systems many times larger than the one built at ORNL. Since tension must increase much faster than system size, there will be a practical limit on size. Where this limit lies, depends on

Table 4.4 7x19 Steel Wire Rope Scaling Parameters

Stiffness (lb/in)	***A***	***n***
343	0.0163	1.639
518	0.0231	1.649
781	0.0548	1.635
1179	0.0814	1.636
2683	0.1205	1.638
4047	0.1796	1.638
6105	0.2700	1.636
9211	0.4038	1.635
13895	0.5920	1.640
20962	0.8164	1.669
31623	1.1400	1.701

how much power use, and what size motors are considered reasonable and economical, and what weight limits on structural components are necessary. Nonetheless, scaling along a constant stiffness contour will be tension limited.

There are two ways to get around this dilemma that could be areas of future research on the SkyBAAM system. First, a method to cope with lower stiffness at larger sizes could be developed. This could be done through control strategies for compliant actuators, such as a command shaping control strategy. Another alternative would be to use a macro-micro manipulator strategy, where a high bandwidth micro-manipulator on the end effector can compensate for errors in the low stiffness and low bandwidth cable-driven manipulator. A second way to deal with this limit is to develop new materials that have a higher stiffness-to-weight ratio than steel; for example carbon fiber cables could be used. Currently, carbon fiber cables are limited to static applications that do not need to repeatedly bend over pulleys, so new types of carbon fiber cables would have to be developed for application in SkyBAAM.

To demonstrate how carbon fiber cables would improve the system, a comparison between the two can be made. Assuming a carbon fiber cable would have the same modulus as low-grade fibers, a modulus of 33,000 ksi, and a density of 0.073 $\frac{lb}{in^3}$ is assumed. From here the stiffness with respect to tension can be found in a similar manner as was done for the steel cables. This is plotted in Figure 4.9 alongside stiffness for a 7x19 steel wire rope for three diameters. Diameters for the carbon fiber cables were chosen to have similar asymptotic stiffness as the steel cables. It can be seen, for the diameters and lengths used in this example, the carbon fiber requires roughly $1/7^{th}$ the tension steel does for a given stiffness. In future systems that are many times larger than the system developed at ORNL, there would be significant benefit to developing carbon fiber cables that would be suitable for this application.

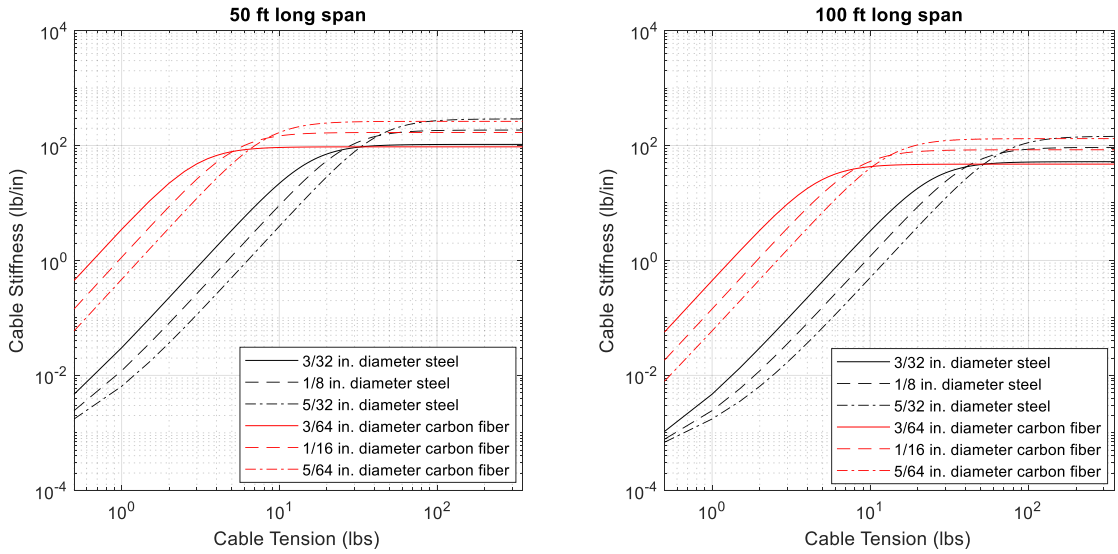

Figure 4.9 7x19 Steel vs. Carbon Fiber Cables

Summary

This chapter analyzes the performance of the SkyBAAM system. First a stiffness index was developed to understand how stiffness changes throughout the workspace. Then singularities were discussed as well as a method for quantifying the workspace of the system. This was then applied to the prototype SkyBAAM system built at ORNL, and the workspace was plotted for this system and stiffness and cable tensions throughout the workspace were plotted and discussed. Finally scaling laws and limitations were discussed as well as well as potential ways of dealing with these limitations.

Chapter Five
RESULTS ON THE PROTOTYPE SYSTEM

Having done analysis of the SkyBAAM system, a prototype system was built at ORNL. The analysis of this system was presented in the previous chapter. Here the system that was built is presented. Also, measurements from that system are presented. Finally, this chapter presents concrete parts printed on the system. The mechanical and electrical design of the physical system is out of the scope of the work done on this thesis, but the physical system is presented for completeness. The mechanical and electrical design, fabrication, and testing of the ORNL SkyBAAM system is not solely the work of the author, but of the whole ORNL SkyBAAM team.

Prototype System

The prototype system built at ORNL is nominally 25’ x 25’ in footprint with a height of 18’. The nominal size of the system built is shown in Figure 5.1, and it uses 1/8” 7x19 steel wire rope for the motion cables and nylon rope for the tension cables.

The system was designed with four base stations that contain the *x*, *z*, *x’*, and *y’*-winders. The *z*-winder is placed on the *y*-station and *z*-cable goes over a pulley at the apex to go down the end effector. An overall view of the fabricated system is shown in Figure 5.2. Here the base stations can be seen as well as the apex that is held up by the overhead crane.

The base station frames are made from welded steel tubing in a pyramidal structure for high structural stiffness. The cable winders and pulleys, and boxes for electronics are attached to these frames. A single spool is used to wind cables on and off for each motion direction. Figure 5.3 shows the *x*-station. Here a single winder in the center of the front plate winds the three *x*-cables. These three cables are wound over pulleys to three exit pulleys. These exit pulleys are free to rotate so that as the cables moves with the end effector, the pulleys are always in line with the cable. The *y*-station is similar, except it has two *y*-cables arranged vertically that wind off a common central spool.

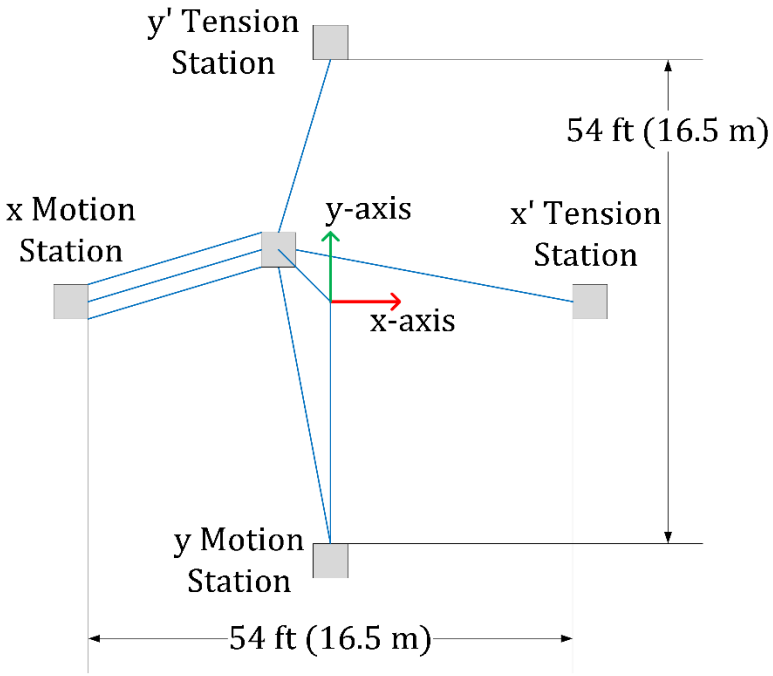

Top View

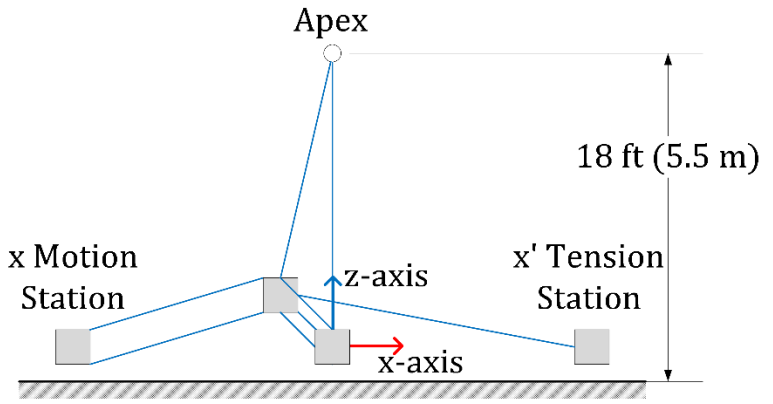

Side View

Figure 5.1 ORNL SkyBAAM Layout

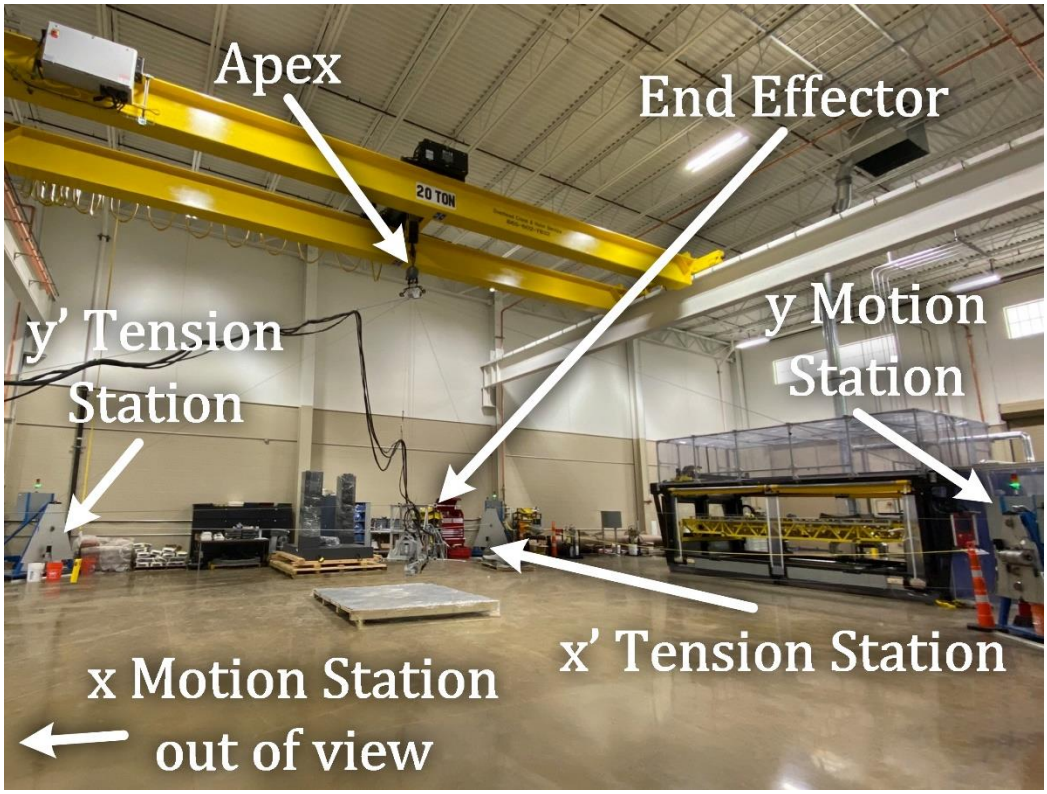

Figure 5.2 ORNL SkyBAAM System

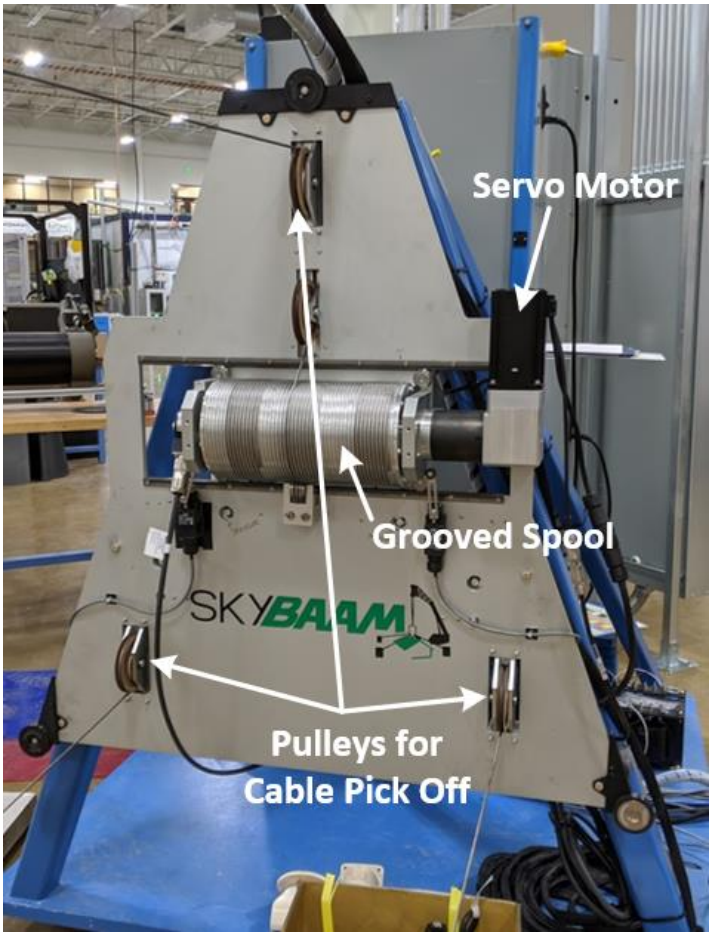

Figure 5.3 X-Station

On the motion cables, it is desirable to accurately control the payout of the cables in and out. Figure 5.4 shows a close up view of the spool on the *x*-station. The spools for motion cables are grooved with the diameter of the cable so that the cables always lie repeatably in the same way. The spool also moves horizontally as cable is wound on and off. This ensures that the exit angle of cable with respect to the spool is always constant. The spools are servo driven with encoder feedback to accurately pay known amounts of cable in and out.

The apex point is held up by the overhead crane. As seen in Figure 5.2 a gantry crane was used, but any type of crane can be used that will provide sufficient capacity. There is a pulley on the apex that routs the *z*-cable back down to the ground, where it is would on a cable winder on the *y* motion station. The apex position is constrained by four stay cables that are anchored to the base stations. Since these stay cables constrain the apex, compliance in the crane that is holding up the apex is not an issue; all of the rigidity of the apex position is supplied by the stay cables. In fact, it is desirable to have some compliance between the apex and the crane so that the crane does not put excessive tension on the stay cables as it pulls up against them. In the system built at ORNL there are springs between the apex and the connection to the crane hook to provide this compliance.

An interesting and exotic alternative to using a crane to suspend the apex, would be to use a large balloon, such as a weather balloon. Since the stay cables provide the constraint needed, only an upward force is needed, and a balloon could provide this. Of course, with a balloon, weather concerns become greater, and the system could not be run in strong winds.

Controls Overview

In [9] the control strategy for the SkyBAAM has been reported. While control development of SkyBAAM is not within the scope of this thesis work, a high-level overview is included here for completeness. The controls for SkyBAAM were primarily developed by Dr. Brian Post and Dr. Joshua Vaughan.

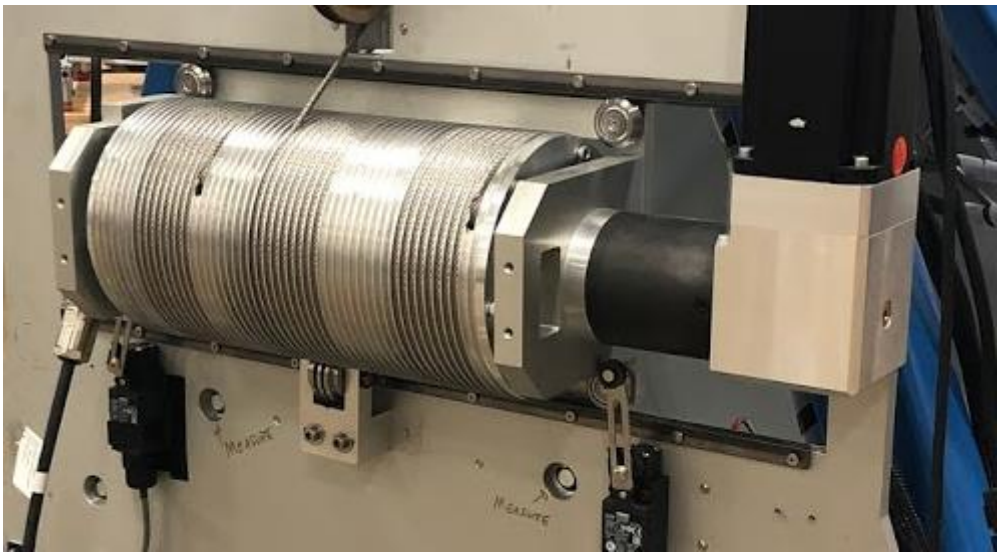

Figure 5.4 X-Spool

Figure 5.5 from [9] shows the control scheme. The commanded cartesian position is $Y_d(s)$. The inverse kinematics (shown as *IK* in figure) compute the cable lengths. The cable lengths are fed into a low-level closed-loop controller, G_i, with feedback from the encoders on the winding drums. The actual cable lengths measured from the encoders, $L(s)$ are fed into the forward kinematics (shown as *FK* in figure) to give an estimated cartesian position, $Y_{est}(s)$. This position is then fed back to generate the estimated error signal. Future work will include using a laser tracker to actively measure the end effector location so that the true end effector position can be fed back to generate the error signal instead of the estimated position.

Repeatability

In [9], measurements of repeatability were done on the SkyBAAM system to quantify the positioning performance of the system. These results are summarized here. A set of points in the workspace was chosen, and the end effector was repeatedly moved to these points from different areas of the workspace, and the position was measured with a Leica AT960 laser tracker. The maximum deviation between measured locations for each move to a location was recorded, and this was repeated for every point in the set. This was done for a 100 ft^3 volume in the workspace and a 600 ft^3 volume in the workspace.

The results of this are plotted in Figure 5.6 which is repeated from [9]. For the 100 ft^3 volume the maximum deviation was 0.0675 inches while the average error was only 0.0322 inches. The system was highly repeatable in this area of the workspace. For the larger 600 ft^3 volume. Here the maximum error was much larger at 0.2451 inches. However, the average error was only 0.0643 inches. It is not surprising that in this case some of the points had a larger deviation, since the large volume had points closer to the extreme values of the workspace. These measurements were made without any closed loop feedback on the end effector location. By using a laser tracker to give feedback on the end effector location, these values could be tightened up significantly.

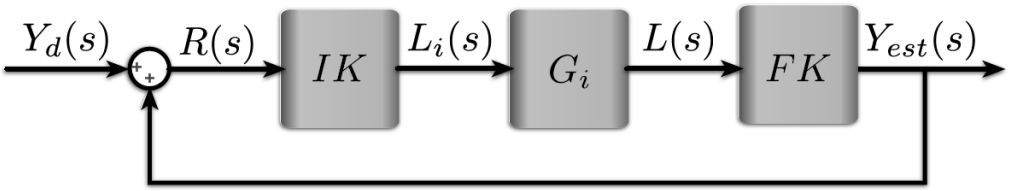

Figure 5.5 Open Loop Control Diagram [9]

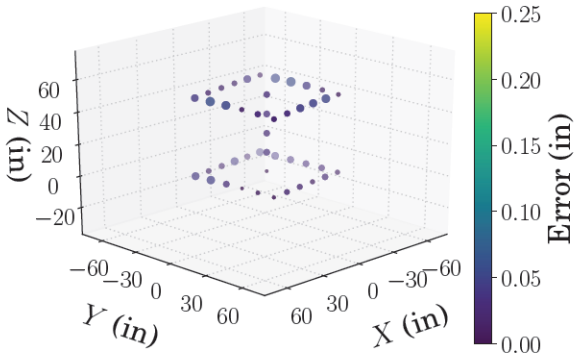

(a) OVER A 100ft^3 WORKSPACE

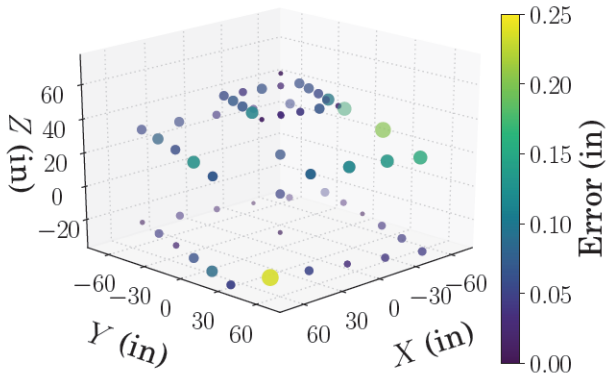

(b) OVER A 600ft^3 WORKSPACE

Figure 5.6 Open Loop Repeatability [9]

This level of error is acceptable considering the size object to be printed and the size of the extrusion bead width. This system is used to print beads around two inches wide, and even the maximum error is nearly an order of magnitude smaller than the bead width.

Natural Frequencies

Natural Frequencies of the system were measured in [9]. A modal hammer with an accelerometer on the end effector was used to measure the response to an impulse (hammer hit). From this data natural frequencies and damping ratios can be calculated. The details of the procedure to calculate these are not reported here. This was done in both the *x* direction and the *y* direction for several end effector positions and the mode with the lowest frequency was extracted. The natural frequencies and calculated damping ratios are plotted in Figure 5.7 as repeated from [9]. For these tests, the end effector was at x=0 and y=0 and the *z*-height was varied as plotted on the graph. As can be seen natural frequencies were in the 3-6 Hz range and damping ratios were reasonably high, being from 0.25 to 0.5. For lower positions the natural frequency is higher because the cables are more in line with the *x* and *y* directions, while the frequency trends down for higher positions as the cables have more angle and consequently less stiffness in the *x*-*y* plane.

To compare these measured values to the stiffness model developed above, natural frequencies can be calculated using the stiffness matrix that was found previously by using the classical eigenvalue method for finding natural frequencies and mode shapes for a multi-degree of freedom (MDOF) system. This method is described in texts such as [32] and [33] and many others, so the full derivation will not be given here.

If there is no applied loading (i.e. free vibration) and the system has negligible damping, the equation of motion of a MDOF system is:

$$M\ddot{\boldsymbol{x}} + K\boldsymbol{x} = 0$$

where M is the mass matrix, K is the stiffness matrix and $\boldsymbol{x}$ is the position vector. The solution is of the form:

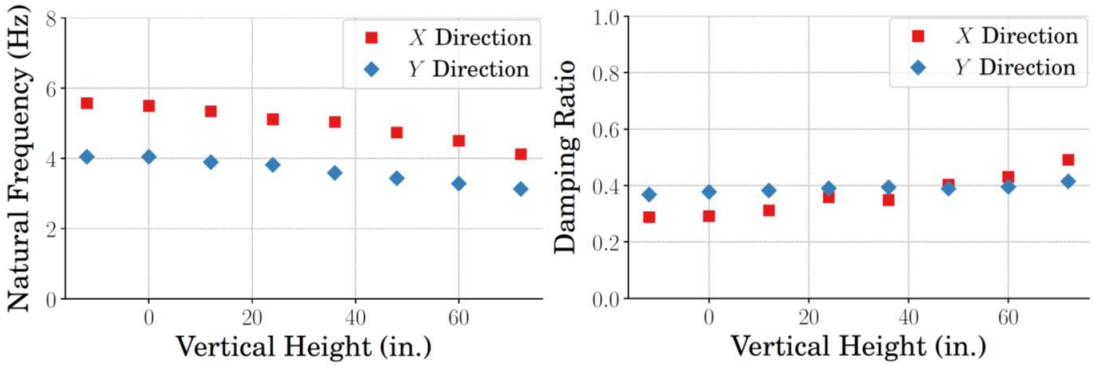

Figure 5.7 Natural Frequencies and Damping [9]

$$\boldsymbol{x}(t) = \boldsymbol{u}e^{i\omega t}$$

where $\boldsymbol{u}$ is the mode shape and ω is the natural frequency. The mode shapes and natural frequencies can be found from the dynamical matrix A where

$$A = K^{-1}M$$

The mode shapes are the eigenvectors of A, and the natural frequencies (in rad/s) for each mode shape are the square root of the corresponding eigenvalues.

To calculate the natural frequencies and mode shapes, the stiffness and mass matrices must be known. The stiffness matrix for SkyBAAM has already been derived. The mass matrix can be approximated by assuming 150 lbm evenly distributed in a rectangular solid 24 in. x 24 in. x 36 in.

The data taken above was measured with the SkyBAAM base stations in the configuration discussed in the previous chapter. The tension cables were both set to 250 lbf. For the theoretical natural frequencies, the stiffness matrix was calculated at each position with 250 lbf on the tension cables. The natural frequencies and mode shapes were calculated from this. Then the lowest frequency mode in both the *x* direction and *y* direction was identified. The calculated natural frequencies for these modes are plotted in Figure 5.8 alongside the measured data. It will be noted that there is a small difference between the calculated and measured frequencies. This difference is probably due to not including damping in the theoretical natural frequencies as well as error in the estimation of the mass matrix. However, the agreement between the calculated and measured natural frequencies is very good, and both the measured data and the calculated data follow the same trend. These results increase confidence in the model that has been derived for SkyBAAM herein.

Printed Parts

This thesis has focused on the SkyBAAM motion platform and has not delved into the challenges of depositing concrete or cement with the system. However, significant work

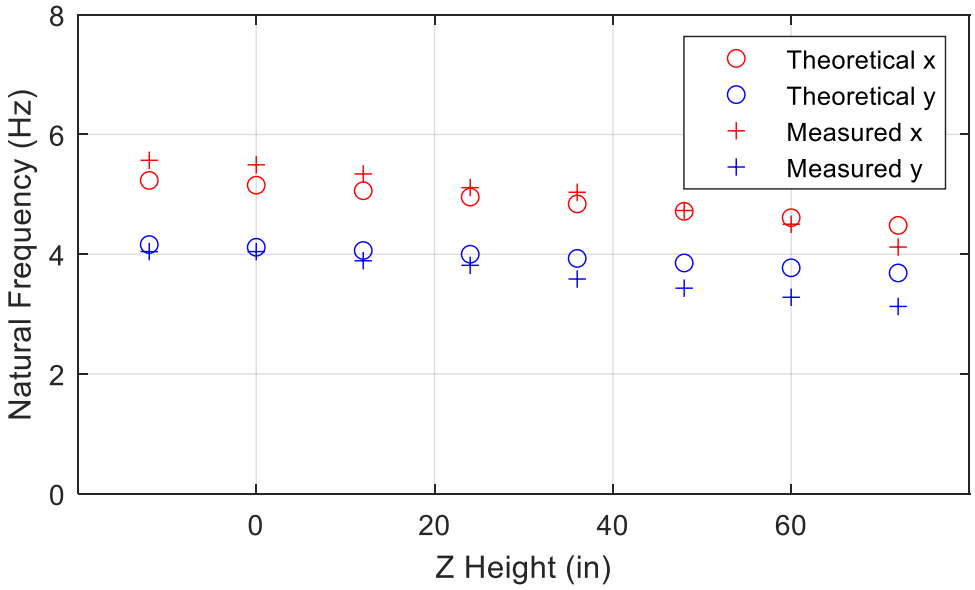

Figure 5.8 Measured vs. Theoretical Natural Frequencies

was put into developing extruders and pumping systems for extruding concrete at the end effector. In this section a summary of the printing that was done on SkyBAAM is given. This demonstrates that the SkyBAAM system functioned as anticipated and was able to achieve the design goal of printing large parts. It will be noted that in some of the photographs the cables are blue. This is because when the system was first brought on line Dyneema cables were used instead of steel wire rope since that was easier to work with. The motion cables were later replaced with 1/8" 7x19 steel wire rope as discussed previously. The tension cables were replaced with a high stretch nylon rope to make it easier to control the tension accurately.

The first print on SkyBAAM was a three-foot diameter circle one layer wide and eight layers tall. This is shown in Figure 5.9. Subsequent prints on SkyBAAM were of larger size and more geometrical complexity.

Another early print on SkyBAAM was a much larger and taller cylinder. This print was approximately 10 ft. in diameter and 5 ft. tall. It was printed over the course of two days. The first day a base was printed that was backfilled with rebar and concrete. On the second day of printing the rest of the cylinder was printed on this base. This print is shown in the SkyBAAM work envelope in Figure 5.10.

An example of a print done when the extruder and material delivery system were more developed is the EMPOWER wall [9]. This is a printed wall that was made to demonstrate how energy saving can be achieved with printed structures. During printing, pipes were emplaced in the structure that could later be used to pipe fluid through to control the heat transfer characteristics of the wall. The final EMPOWER wall was 8 ft. long and 6 ft. tall. A picture of the Empower wall during printing is shown in Figure 5.11.

Printing Outside

In November 2020 a demonstration of the deployability for SkyBAAM was done. The base stations were secured in 10 ft. shipping containers for easy transportation and setup, as well as providing weatherproofing. The base stations were moved to an outdoor location, and a

Figure 5.9 First SkyBAAM Print

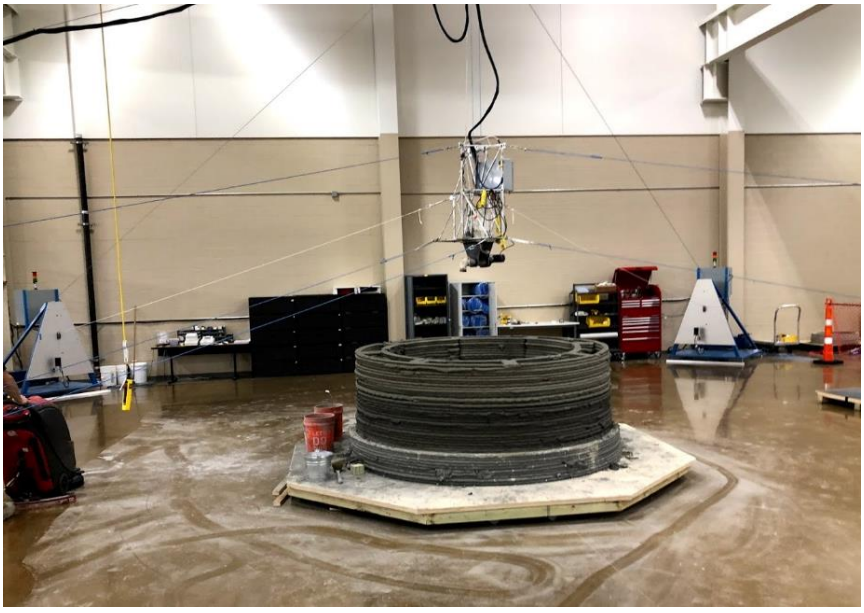

Figure 5.10 Early SkyBAAM Print

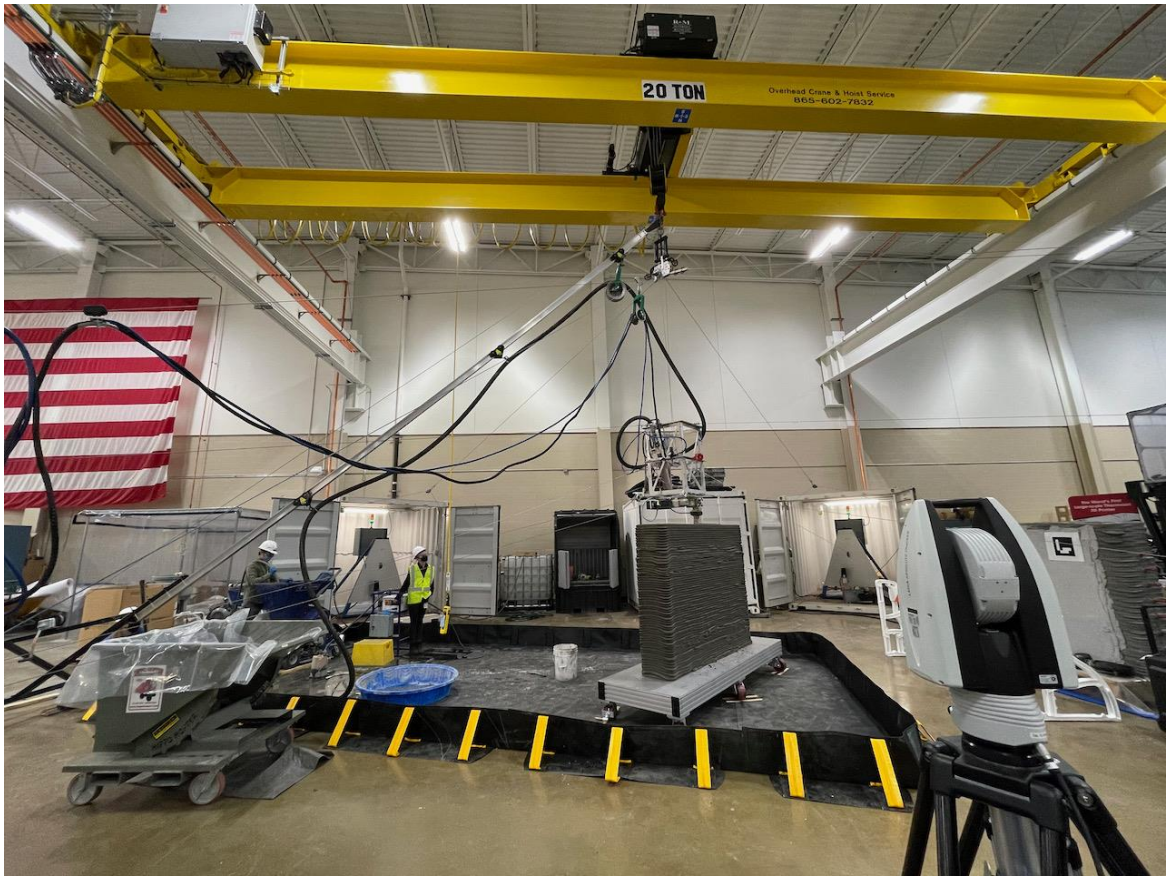

Figure 5.11 EMPOWER Wall Print

large forklift was used as the crane to suspend the apex point. This is shown in Figure 5.12. A roughly 5000 lb part was printed in this setup.

Summary

This chapter discussed the prototype SkyBAAM system built at ORNL. There was discussion of the mechanical design as well as the controls. Repeatability measurements were given as well as measurements of the natural frequencies and comparison to theoretical natural frequencies. Finally, examples of parts printed on the system were shown.

Figure 5.12 SkyBAAM Outdoor Setup

Chapter Six

CONCLUDING OBSERVATIONS

Overall Summary

In this thesis the design and analysis of a cable-driven manipulator for additive manufacturing is presented. The design philosophy for the SkyBAAM cable-driven motion platform is discussed and how this led to the cable configuration that was used. The SkyBAAM system was built at ORNL and has been successfully used to print numerous concrete parts and is continuing to be used in the development of concrete additive manufacturing at ORNL.

This thesis covers certain aspects of the development of the SkyBAAM motion platform. This starts with deriving the forward and inverse kinematics of the system. On a parallel system such as this the inverse kinematics are simple while the forward kinematics are quite complex.

The tension effects on the cables are examined in some detail. Since the stiffness of an individual cable is affected by the tension on a cable model for the stiffness of a cable with respect to tension is derived. This model shows that the cable stiffness approaches an asymptotic stiffness that is governed by the elastic properties of the cable. Keeping cable tensions above a threshold value will keep the stiffness close to this maximum asymptotic stiffness. In order to keep the system stiffness high in an efficient manner, a method is derived for controlling the system tension in a way that keeps cables above their required threshold stiffness while minimizing unnecessary tension in the system. System tension is controlled through the use of two tensioning cables. Changing the tension in these two cables manipulates the tension vector applied to the system.

The six DOF stiffness matrix for the end effector is also derived. In order to have a single stiffness measurement to use in design, a stiffness index is developed. This is done by using eigenvalues to quantify the minimum *x-y* plane stiffness of the deposition tip or nozzle.

The workspace was is analyzed through the lens of both tension and singularities. Points are considered to be in the workspace if the system is reasonably able to achieve the required tension values for each cable, and if the end effector is reasonable far from a singularity. What is considered reasonable for tensioning and distance from a singularity can be tuned by the designer depending on the workspace requirements and what allowable requirements are on mechanical components and energy usage.

These analysis techniques are applied to the prototype SkyBAAM system built at ORNL. This includes finding the workspace of the system, and quantifying the tension required throughout the workspace. The stiffness index is also evaluated throughout the workspace. Natural frequencies of the system are calculated using the derived stiffness matrix for the end effector. This is compared against measured data. Close correlation between the predicted and measured natural frequencies increase confidence in the model derived for SkyBAAM.

A scaling analysis was done on the SkyBAAM system. This shows that to scale up the system and keep the stiffness equivalent the tensions must scale up by a power of 1.65. This obviously creates problems for future work of scaling this system up to much larger sizes needed for printing buildings or other similar objects.

Open loop repeatability of the prototype SkyBAAM system built at ORNL was measured and was found throughout the workspace to be significantly smaller that the size of beads the system is meant to deposit. This shows the suitability of the system for the type of deposition it is intended for.

Lessons Learned

The analysis of the SkyBAAM system as presented in this thesis led to several significant lessons learned about SkyBAAM and its suitability for AM of concrete structures.

One of the primary issues that is noted herein is the shape of the workspace. It is a conical or “circus tent” shaped volume. This does not easily lend itself to the rectangular prismatic shape of most buildings and concrete structures. As discussed previously it is possible that

certain things could be done to increase the workspace. This includes making the base stations move vertically upward during the printing process, as well as adding more base stations to increase the maximum footprint of the workspace.

A second important lesson is the scaling limitations. Since the required tension for the cables scales to the power of 1.65 instead of linearly, larger systems will hit tension limits or will require very large mechanical components and use large amounts of energy. There are routes for future research that could combat this scaling limit, as discussed previously.

A third and more favorable lesson is that the SkyBAAM system exhibits good stiffness as seen in both theoretical analysis and empirical testing. Testing also showed that the system has relatively high damping ratios which is good for inhibiting the excitation of vibrational modes.

A fourth lesson learned is that the system has good open loop repeatability. Further work will be done on closing the loop on position and this will only serve to further improve the system accuracy. However, even the open loop repeatability is good enough for the types of AM processes the system is designed for.

Future Research

There are a number of areas for future research to improve the SkyBAAM motion platform. This includes addressing some of the issues that have been mentioned as well as opening up new lines of inquiry.

The first is adding closed loop control to the end effector position using the laser tracker. This will allow for better positional accuracy of the deposition head in space.

To address the workspace limitations the possibility of moving the base stations upward during the printing process could be examined. Also, the possibility of adding more base stations could be examined.

Several options are also open for addressing the scaling limitations. First, carbon fiber cables could be developed for use in this type of motion application. These cables would have a better stiffness to weight ratio than steel, and thus would require less tension. As shown previously, carbon fiber cables result in a significant decrease in required tension. Secondly a micro-macro manipulator approach could be taken. Here a lower stiffness is accepted for the end effector, allowing cables tensions to be lower. This will decrease the bandwidth and accuracy of the system. However, to compensate for this, a high bandwidth micro manipulator is placed on the end effector that will move deposition head small amounts to compensate for error in the macro end effector position. Both of these ideas for reducing the scaling limitations are still purely conceptual at this point and further research would be warranted.

A final area for future research is optimization of base station position. In the present work analysis was done to find the workspace given a known location of the base stations and apex pulley. The inverse of this would be more useful in a real-world application. Given an object that needs to be printed as well as constraints on where the base stations can go, where should the base stations be placed? This would likely require some complex optimization algorithm or the use of artificial intelligence. For example, a genetic optimization algorithm could find a configuration that met the workspace requirements and minimized some cost function such as total footprint. Solving this problem will likely be necessary to allow for commercial implementation of the system since contractors will need an easy was to determine base station placement.

Closing Remarks

In closing, this thesis detailed important aspects of the design, analysis and testing of the SkyBAAM motion platform for additively manufacturing concrete structures. This system was successfully used to print large concrete objects. However, there are certain limitations to the system, namely an oddly shaped workspace and difficulties that will come with scaling the system out to larger sizes. Future research may mitigate these issues and possible areas for future research are outlined here. Even so there are many strengths to

this system. It is easily deployable, as shown in outdoor deployment and demonstrations that were done. It also shows good motion control for the given application. The potential for a very large workspace is also present, although there are certain challenges to this that must be overcome in future research.

The ORNL SkyBAAM system is a successful demonstration of a mid-scale, deployable motion platform for AM. It is the hope of the author that this system will be a step towards the goal of easily deployable AM systems that can ultimately be used in commercial construction applications. The analysis presented here can be used to help aid the design of future systems with the SkyBAAM architecture.

LIST OF REFERENCES

[1] R. F. Lind, "Automated Freeform Construction," in *Proceedings of Solid Freeform Fabrication Symposium*, Austin, Texas, 2009.

[2] R. Buswel, "Freeform Construction: Mega-scale Rapid Manufacturing for Construction," *Automation in Construction*, vol. 16, no. 2, pp. 224-231, 2007.

[3] J. J. Biernacki, J. W. Bullard, G. Sant, K. Brown, F. P. Glasser, S. Jones, T. Ley, R. Livinston, L. Nicoleau, J. Olek, F. Sanchez, Shahsavari, P. E. Stutzman, K. Solbolev and T. Prater, "Cements in the 21st Century: Challenges, Perspectives, and Opprotunities," *Journal of the American Ceramic Society*, vol. 100, pp. 2746-2773, 2017.

[4] B. Koshnevis, D. Hwang, K. Yao and Z. Yeh, "Mega-scale Fabrication by Cotour Crafting," *International Journal of Industrial and SYstem Engineering*, vol. 1, no. 3, pp. 301-302, 2006.

[5] J. Jagoda, Diggs-McGee, M. Kreiger and S. Schuldt, "The Viability and Simplicity of 3D-Printed Construction: A Military Case Study," *Infrastructures*, vol. 5, no. 35, 2020.

[6] National Aeronautics and Space Administration, "NASA's Centennial Challenges: 3D-Printed Habitat Challenge," 21 1 2020. [Online]. Available: https://www.nasa.gov/directorates/spacetech/centennial_challenges/3DPHab/about.html. [Accessed 1 5 2020].

[7] R. Buswell, W. R. Lear de Silva, S. Jones and J. Dirrenberger, "3D printing using concrete extrusion: A roadmap for research," *Cement and Concrete Research*, vol. 112, pp. 37-49, 2018.

[8] F. Bos, R. Wolfs, Z. Ahmed and T. Salet, "Additive manufacturing of concrete in construction: potentials and challenges of 3D concrete printing," *Virtual and Physical Prototyping*, vol. 11, no. 3, pp. 209-225, 2016.

[9] C. Atkins et al., "Construction-Scale Concrete Additive Manufacturing and Its Application in Infrastructure Energy Storage," in *Proceedings of the ASME 2020*

International Mechanichal Engineering Congress and Exposition, Portland, OR, 2020.

[10] P. Chesser et al., "Fieldable Platform for Large-Scale Deposition of Concrete Structures," in *Proceedings of Solid Freeform Fabrication Symposium*, Austin, TX, 2018.

[11] C. Gosselin, "Cable-Driven Parallel Mechanisms: State of the Art and Perspectives," *Bulletin of the JSME*, vol. 1, no. 1, pp. 1-17, 2014.

[12] S. Qian, B. Zi, W.-W. Shang and Q.-S. Xu, "A Review on Cable-Driven Parallel Robots," *Chinese Journal of Mechanical Engineering*, vol. 31, no. 66, 2018.

[13] R. Bostleman, J. Albus, N. Dagalakis and A. Jacoff, "RoboCrane Project: An Advanced Concept for Large Scale Manufacturing," in *Proceedings of the AUVSI Conference*, Orlando, FL, 1996.

[14] R. Thompson and M. Blackstone, "Three-dimensional moving camera assembly with an informational cover housing". US Patent US6873355B1, 7 August 1998.

[15] D. Li and Z. Pan, "The Five-hundred-meter Aperture Spherical Radio Telescope project," *Radio Science*, no. 51, pp. 1060-1064, 2016.

[16] N. A. Parameswaran, I. Chornyy, F. de Saint Victor, D. Kedrowski, R. Owen and E. Schmieman, "Massive and Unique," *Lift and Hoist International*, September/October 2012.

[17] P. Bosscher, R. William II, L. S. Bryson and D. Castro-Lacouture, "Cable-Suspended Robtic Contour Crafting System," *Automation in Construction*, vol. 17, no. 4, pp. 45-55, 2008.

[18] E. Barnett and C. Gosselin, "Large-Scale 3D Printing with a Cable Suspended Robot," *Additive Manufacturing*, vol. 7, pp. 27-44, 2015.

[19] T. Bruckmann, H. Mattern, A. Spengler, C. Reichert, A. Malkwitz and M. Konig, "Automated Construction of Masonry Buildings using Cable-Driven Parallel Robots," in *ISARC*, Auburn, AL, 2016.

[20] I. Vukorep, "Autonomous Big-Scale Additive Manufacturing Using Cable-Driven Robots," in *ISARC*, Taipei, Taiwan, 2017.

[21] H. Hong, J. Ali and l. Ren, "A Review on Topological Architecture and Design Methods of Cable-Driven Mechanism," *Advances in Mechanical Engineering*, vol. 10, no. 5, pp. 1-14, 2018.

[22] L. Gagliardini, S. Caro, M. Gouttefarde and A. Girin, "Discrete Reconfiguration Planning for Cable-Driven Parallel Robots," *Mechanism and Machine Theory*, vol. 100, pp. 313-337, 2016.

[23] H. Liu, C. Gosselin and T. Laliberté, "Conceptual Design and Static Analysis of Novel Planar Spring-Loaded Cable-Loop-Driven Parallel Mechanisms," *Journal of Mechanisms and Robotics,* vol. 4, no. 2, 2012.

[24] S.-R. Oh and S. Agrawal, "Cable Suspended planar Robots with Redundant Cables: Controllers with Positive Tension," *IEEE Transactions on Robotics,* vol. 21, no. 3, pp. 457-465, 2005.

[25] E. Weisstien, "Catenary," Wolfram Alpha, [Online]. Available: http://mathworld.wolfram.com/Catenary.html.

[26] Loos & Co. Inc., "How to Calculate Wire Rope and Cable Stretch," 2 7 2010. [Online]. Available: http://blog.loosco.com/bid/42817/How-to-Calculate-Wire-Rope-and-Cable-Stretch. [Accessed 30 12 2020].

[27] S. Behzadipour and A. Khjapour, "Stiffness of Cable-based Parallel Manipulators with Application to Stability Ayalysis," *Journal of Mechanical Design*, pp. 303-310, 2006.

[28] J.-P. Merlet, Parallal Robots, Dordrecht: Springer, 2006, p. 260.

[29] H. Wei, Y. Qiu and J. Yang, "An Approach to Evaluate Stability for Cable-based Parallel Camera Robots with Hybrid Tension-stiffness Properties," *Int J Adv Robot Syst*, vol. 12, no. 158, 2015.

[30] Y. Su, Y. Qui and L. Peng, "Optimal Cable Tension Distribution of the High-Speed Redundant Driven Camera Robots Considering Cable Sag and Inertia Effects," *Advances in Mechanical Engineering*, 2014.

[31] C. Gosselin and M. Grenier, "On the Determination of the Force Distibution in Overconstrained Cable-Driven Parallel Mechanisms," *Meccanica,* vol. 46, pp. 3-15, 2011.

[32] J.-S. Wu, Analytical and Numerical Methods for Vibration Analyses, Singapore: John Wiley & Sons Singapore Pte. Ltd., 2013.

[33] S. G. Kelly, Mechanical Vibrations, Stamford, CT: Cengage Learning, 2012.

[34] L. Sciaviccio and B. Siciliano, Modeling and Control of Robot Manipulators, London: Springer, 1996.

APPENDIX

MATLAB Code

The MATLAB code is divided into several programs. The first is a SkyBAAM class. This does the bulk of the heavy lifting and the other programs call this class. The other programs do specific things such as finding the limits of the workspace. Comments in the code provide further explanation.

SkyBAAM.m

This is the SkyBAAM class. All other code uses this.

```
classdef SkyBAAM < handle
    %SkyBAAM - This class performs calulations relating to SkyBAAM. An
    %instance of the class has associated calibration data that is set
when
    %constructing an instance. This class can be used to calculate
forward
    %and inverse kinematics, find the jacobian, find necessary tension
    %values, find end effector stiffness and mode shapes. It is
envisioned
    %that this class will be used for taks such as finding SkyBAAM
tensions
    %or performance over a region or other such tasks.

    properties
        CableWeights %Vector of cable weights. Units: lb/in.
        CableDiameters %Vector of cable diameters. Units: in.
        cm
    end
    properties (SetAccess = private)
        Pose %Current SkyBAAM position is a vector of length 3
        Calibration %Calibration data. Units: in.
        Jacobian %Jacobian for current SkyBAAM position
        CableTensions %Vector of cable tensions. Units: lbs.
        CableLengths %Vector of cable lengths. Units: in.
        CableDirections %Unit vectors of cable directions
        CableStiffnesses %Stiffness of individual cables
        EFstiffness %Stiffness of the end effector for forces and
moments at the end effector origin
        EFweight %End Effector Weight. Units lbs.
        EFmass %End Effector Mass. Units slugs
        TensionMargin
        Lambda
        x_min_Tension
        y_min_Tension
    end

    methods
        function obj = SkyBAAM(R,G)
        %SkyBAAM Constructs an instance of the SkyBAAM class.
        %   Syntax: obj = SkyBAAM(R,G)
        %   Calibration Data must be provided to create an instance
```

```
        %   of SkyBAAM.
        %   R is a 3x8 matrix that holds the location of
        %   the cable points on the end effector relative the the end
        %   effector coordinate system. G is a 3x8 Matrix that
        %   holds the location of the ground winders relitive to the
global
        %   Coordinat system.
        %
        %   R and G must be in inches

            if prod(size(R) == [3 8]) && prod(size(G) == [3 8])
                s = struct('R',R,'G',G);
                obj.Calibration=s;
            else
                error('R and G must be 3x8 Matricies')
            end

        end

        function [] = SetPose(obj,p)
            %SetPose sets the position of the end effector of an
instance
            %   of the SkyBAAM class.
            %   obj.SetPose(p) sets the current position to p.
            %
            %   p is a vector of length 3 with the x y z position of
the
            %   end effector
            %
            %   When the position is set using SetPose the inverse
            %   kinematics are automaticaly calculated and the cable
            %   lengths are stored in the CableLengths property as a
            %   vector. The Jacobian is also authomatically calculated
and
            %   stored in the Jacobian property

            if prod(size(p) == [3 1]) || prod(size(p) == [1 3])
                if prod(size(p) == [1 3])
                    p = p';
                end
                obj.Pose = p;
                [obj.CableLengths, obj.CableDirections] =
InverseKinematics(obj,p);
                obj.Jacobian = FindJ(obj);
                obj.CableTensions=[];
                obj.CableStiffnesses=[];
                obj.TensionMargin=[];

            else
                error('Pose must have length of 3');
            end
        end
```

```
        function [L, U] = InverseKinematics(obj,pose)
            %InverseKinematics finds the cable lengths for a given end
            %   effector position.
            %
            %   [L, U] = obj.InverseKinematics(p) find the cable
lengths of
            %   SkyBAAM, L, and also the unit vectors of the cables, U,
at
            %   point p. p is a vector of length 3
            %
            %   L = obj.InverseKinematics(p) returns only the lengths
of the
            %   cables.
            %
            %   L is in inches
            %
            %   Inverse Kinematics does not set the length or current
            %   position of the SkyBAAM object. When SetPose is used
            %   Inverse Kinematics are authomatically done and the
object's
            %   properties are updated.

            if prod(size(pose)==[3 1])
                Rg = obj.Calibration.R + pose*[1 1 1 1 1 1 1 1];
%Position of printhead cable points in global coordinates
                U = obj.Calibration.G-Rg;
                L = vecnorm(Rg-obj.Calibration.G);
                for i = 1:8
                   U(:,i) = U(:,i)/L(i);
                end
                % U = matrix of unit vector for cables, L = matrix of
cable lengths
            else
                error('Pose must be 3x1');
            end
%             obj.Calibration.G(1,6)=pose(1);
%             obj.Calibration.G(2,6)=pose(2);
        end

        function J = FindJ(obj)
            %FindJ finds the Jacobian of a SkyBAAM object at its
current
            %   position.
            %   J = obj.FindJ returns the Jocobian at the objects
current
            %   position.
            %
            %   FindJ does not set current properties of the SkyBAAM
            %   object. When SetPose is used the Jacobian
authomatically
            %   found and the object's properties are updated.

            A = zeros(6,8); %A = static equilibrium matrix
            U = obj.CableDirections;
```

```
            R = obj.Calibration.R;
            for i = 1:8
              A(:,i) = [U(:,i); cross(R(:,i),U(:,i))];
            end
            J=A'; %Jacobian
        end

        function pForward = ForwardKinematics(obj,L)
            %ForwardKinematics finds the cable lengths for a given end
            %   effector position.
            %
            %   p = obj.forwardKinematics(L) returns the end effector
            %   position for the vector of cable length L. L is vector
of
            %   length 6.
            %
            %   ForwardKinematics does not update the properties of the
            %   SkyBAAM object. If the given cable lengths do not yield
a
            %   valid position, then ForwardKinematics will throw an
error.

            if prod(size(L) == [1 6]) || prod(size(L) == [6 1])
                if L(1)~=L(2) || L(2)~=L(3) || L(4)~=L(5)
                    error('X and Y stations must have equal cable
lengths')
                end
                R = obj.Calibration.R;
                G = obj.Calibration.G;

                 %% Peter's Solution
%
%                 a1 = 2*(R(1,1)-G(1,1));
%                 b1 = 2*(R(2,1)-G(2,1));
%                 c1 = 2*(R(3,1)-G(3,1));
%                 d1 = L(1)^2 - (a1^2 + b1^2 + c1^2)/4;
%
%                 a2 = 2*(R(1,4)-G(1,4));
%                 b2 = 2*(R(2,4)-G(2,4));
%                 c2 = 2*(R(3,4)-G(3,4));
%                 d2 = L(4)^2 - (a2^2 + b2^2 + c2^2)/4;
%
%                 a3 = 2*(R(1,6)-G(1,6));
%                 b3 = 2*(R(2,6)-G(2,6));
%                 c3 = 2*(R(3,6)-G(3,6));
%                 d3 = L(6)^2 - (a3^2 + b3^2 + c3^2)/4;
%
%
%                 e1 = (a3*(c2-c1)+a2*(c1-c3)+a1*(c3-c2))/(b3*(c1-
c2)+b1*(c2-c3)+b2*(c3-c1));
%                 f1 = (c3*(d2-d1)+c2*(d1-d3)+c1*(d3-d2))/(b3*(c1-
c2)+b1*(c2-c3)+b2*(c3-c1));
%                 e2 = -(a3*(b2-b1)+a2*(b1-b3)+a1*(b3-b2))/(b3*(c1-
c2)+b1*(c2-c3)+b2*(c3-c1));
```

```
%                   f2 = -(b3*(d2-d1)+b2*(d1-d3)+b1*(d3-d2))/(b3*(c1-
c2)+b1*(c2-c3)+b2*(c3-c1));
%
%
%                   g1 = 1 + e1^2 + e2^2;
%                   g2 = a1 + b1*e1 + c1*e2 + 2*e1*f1 + 2*e2*f2;
%                   g3 = -d1 + b1*f1 + f1^2 + c1*f2 +f2^2;
%
%
%                   px = (-g2 - sqrt(g2^2-4*g1*g3))/(2*g1)
%                   py = e1*px+f1
%                   pz = e2*px+f2
%
                   %%

                  a1 = (R(1,1)-G(1,1));
                  b1 = (R(2,1)-G(2,1));
                  c1 = (R(3,1)-G(3,1));
                  d1 = L(1)^2 - a1^2 - b1^2 - c1^2;

                  a2 = (R(1,4)-G(1,4));
                  b2 = (R(2,4)-G(2,4));
                  c2 = (R(3,4)-G(3,4));
                  d2 = L(4)^2 - a2^2 - b2^2 - c2^2;

                  a3 = (R(1,6)-G(1,6));
                  b3 = (R(2,6)-G(2,6));
                  c3 = (R(3,6)-G(3,6));
                  d3 = L(6)^2 - a3^2 - b3^2 - c3^2;

                  M = 2*[a1-a3 b1-b3 c1-c3;
                      a2-a3 b2-b3 c2-c3];

                  b = [d1-d3;
                      d2-d3];

                  H1 = null(M);
                  P1 = pinv(M)*b;

                  search = 1;
                  v = -1000;
                  delta = .01;
                  iteration = 0;

                  while search %Newton method to find root1
                      pForward=P1+H1*v;
                      value1 = sqrt( (pForward(1)+a1)^2 + ...
                              (pForward(2)+b1)^2 + (pForward(3)+c1)^2 )-
L(1);
                      if abs(value1)>.00001
                          pForward2=P1+H1*(v-delta);
                          value2 = sqrt( (pForward2(1)+a1)^2 + ...
```

```
                            (pForward2(2)+b1)^2 + (pForward2(3)+c1)^2
)-L(1);
                        slope = (value1-value2)/delta;
                        v = v - value1/slope;
                        iteration = iteration + 1;
                        if iteration>1000000
                           error('Forward Kinematics does not
converge!')
                        end
                    else
                        search =0;
                    end
                end




            else
                error('L must be length 6')
            end
        end

        function [] = SelectT(obj,tol,W)
            %SelectT finds the appropriate tensions and sets them in
the
            %   appropriate parameter in the SkyBAAM object. SelectT
chooses
            %   tension values such that catenary sag is minimized by
keeping
            %   all tensions above a minimum required value.
            %
            %   obj.SelectT Sets the tension value with no external
force
            %   other than gravity.
            %
            %   obj.SelectT(W) Sets the tensions with an external
wrench,
            %   W, on the end effector. Dynamic forces on the end
effector
            %   should be included in W. W is 1 column vector of length
6.
            %
            %   If it is not possible to find cable tensions above the
            %   minimum required tension then the cable tensions will
be
            %   set to NaN.
            %
            %   The property TensionMargin is a measure of how much
higher
            %   tensions are than the minimum required tension.
            %
            %   The values of the tensioners are the last 2 values in
the
```

```
            %   field CableTensions that is set with this function.

            if nargin<2
               W = [0 0 0 0 0 0]' ;
               tol=.9; %percent of max stiffness that will be targeted
            elseif nargin <3
               W = [0 0 0 0 0 0]' ;
            end



            if ~prod(size(W)==[6 1])
                error('external wrench must have size of 6 in column
vector')
            end
            if isempty(obj.EFweight) || isempty(obj.CableWeights) ||
isempty(obj.CableDiameters)
                error('System not fully defined')
            end
            A = obj.Jacobian';
            W = W+[0 0 -obj.EFweight 0 0 0]';
            L = obj.CableLengths;
            P = pinv(A)*(-W); %Particular soln to cable tensions
            H = null(A); %Homogenous soln to cable tensions

            %Get Vector of minimum tensions
            tMin = ones(8,1);
            for i = 1:5
              tMin(i) = obj.tensionReq(L(i),...
                  obj.CableWeights(i), obj.CableDiameters(i),tol);
            end
            obj.x_min_Tension=tMin(1);
            obj.y_min_Tension=tMin(4);

            %Find Verticies of feasible space
            V=[];
            s = tMin - P;
            for i = 1:7
                for j = (i+1):8
                    vTest = pinv(H([i,j],:))*s([i,j]);
                    tTest = (P+H*vTest);
                    if (sum( (tTest+.2*ones(8,1)) > tMin) == 8)
                      V = [V vTest];
                    end
                end
            end

            %Find Optimum vertex
            tMag = [];
            if ~isempty(V)
                for i = [1:length(V(1,:))]
                    tTest = P+H*V(:,i);
                    tMag(i) = norm(tTest);
```

```
                end
                [~, loc] = min(tMag);
                v = V(:,loc);
            else
                v=NaN;
            end

            %Set Cable Tensions, set stiffness, set tension margin
            obj.CableTensions = P + H*v;
            obj.EndEffectorK;
            obj.TensionMargin = norm(tMin)/norm(obj.CableTensions);
        end

        function [] = SetT(obj,T,W)
            % SetT is an alternative to SelectT to find the tension
values
            %
            %   SelectT chooses tension values to minimize catenary
sag.
            %   However, SetT finds the tensions on all cables when the
            %   tensioners are set to a given tension value.
            %
            %   obj.SetT Sets the tension value with no external force
            %   other than gravity.
            %
            %   obj.SetT(W) Sets the tensions with an external wrench,
            %   W, on the end effector. Dynamic forces on the end
effector
            %   should be included in W. W is a column vector of length
6.
            if nargin<3
               W = [0 0 0 0 0 0]' ;
            end
            if ~prod(size(W)==[6 1])
                error('external wrench must have size of 6 in column
vector')
            end
            if ~(prod(size(T) == [2 1]) || prod(size(T) == [1 2]))
                error('Two Tensions must be provided')
            else
                A = obj.Jacobian';
                W = W+[0 0 -obj.EFweight 0 0 0]';
                P = pinv(A)*(-W); %Particular soln to cable tensions
                H = null(A); %Homogenous soln to cable tensions
                v = (H([7,8],:))\[T(1); T(2)]-P([7,8],:);
            end
            obj.CableTensions = P + H*v; %Cable tensions caculated
            obj.EndEffectorK
        end

        function [] = show(obj)
            %show visualizes the system represented by the current
SkyBAAM
            %   object
```

```
            %
            %   obj.show creates a figure with the cables plotted

            Rg = obj.Calibration.R + obj.Pose*[1 1 1 1 1 1 1 1];
%Position of printhead cable points in global coordinates
            G = obj.Calibration.G;
            figure
            hold on
            for i = 1:8
               x = [Rg(1,i),G(1,i)];
               y = [Rg(2,i),G(2,i)];
               z = [Rg(3,i),G(3,i)];
               plot3(x,y,z,'k')
            end
            view(3)
            grid on
        end

        function [] = setWeight(obj,w)
            %SetWeight Sets both the end effector weight and mass
            %
            %   objSetWeight(w) where w is the weight in lbs
            %
            %   obj.EFWeight and obj.EFmass are the weight and mass of
the
            %   end effector in lbs and slugs respectivly

            obj.EFweight = w;
            obj.EFmass = w/32.2;
        end

        function [Vsort, Dsort] = modeShapes(obj,M)
            %ModeShapes finds the mode shapes and frequencies for the
            %   current system configuration
            %
            %   [V, F] = obj.modeShapes(M) returns the mode shapes, V,
and
            %   the associated frequencies, F, in Hz
            %
            %   M is a 6x6 matrix.
            %
            %   Units for M are m and kg NOT in and slug


            if ~prod(size(M)==[6 6])
                error('Mass matrix must be 6x6')
            else
                K_ef=obj.EFstiffness*175.13; %change untis to N/m
                %Sytem Matrix
                A=inv(M)*K_ef;
                %eigenvalues and eigenvectors of A
                [V,D]=eig(A); %here V is eigenvectors and diagonal of D
is eigenvalues
```

```
            %Sort eigen-values and eigen-vectors
            [Dsort, index] = sort(diag(D),'ascend');
            Vsort = V(:,index);
            Dsort = sqrt(Dsort)/(2*3.14159);
        end
    end

    function  k = K(obj,l,w,d,t,G)
    %K finds stiffness of individual cable
    %   Detailed explanation goes here
      if nargin<6
        G = .000014; %for 7x19 Galvanized wire rope
      end
      k_elas = 100 * d.^2 ./ (l .* G);
      k_sag = (3*t.*l.^2.*w.^2 + 24.*t.^3)./(2.*l^3.*w.^2);
      k = 1 ./ ( (1 ./k_sag) + (1 ./k_elas) );
    end


    function [] = elevateMotion(obj,h)
    %Explaination
    %   More

        H = [0 0 h+36;
            0 0 h;
            0 0 h;
            0 0 h+36
            0 0 h;
            0 0 0;
            0 0 0;
            0 0 0]';

        Mask = [1 1 0;
            1 1 0;
            1 1 0;
            1 1 0;
            1 1 1;
            1 1 1;
            1 1 1]';
        obj.Calibration.G = obj.Calibration.G.*Mask;
        obj.Calibration.G = obj.Calibration.G + H;
    end

end

methods (Access = private)

    function tReq = tensionReq(obj,l,w,d,tol)
    %TENSIONREQ finds tension required in an individual cable
    %   Detailed explanation goes here
    G = .000014;
```

```
            t = 0:1:1000;
            kThresh = tol*100*d^2/(G*l);%tol * obj.K(l,w,d,1000);
            cableK = obj.K(l,w,d,t);
            for i = 1:(length(t)-1)
              if (cableK(i) <= kThresh) && (cableK(i+1) > kThresh)
                tReq = t(i);
                break
              end
            end

        end

        function [] = EndEffectorK(obj)
           %Stiffness of individual cables
            for i = 1:8
              obj.CableStiffnesses(i) = ...
                  obj.K(obj.CableLengths(i), obj.CableWeights(i),...
                  obj.CableDiameters(i), obj.CableTensions(i));
            end
            obj.CableStiffnesses(7) = 0;
            obj.CableStiffnesses(8) = 0;
            %stiffness of end effector
            K_ef = zeros(6,6);
            for i = 1:8
              K_ef = K_ef + obj.Kef3D(obj.CableDirections(:,i),...
                  obj.CableStiffnesses(i),obj.CableTensions(i),...
                  obj.CableLengths(i),obj.Calibration.R(:,i));
            end
            obj.EFstiffness = K_ef;

            if ~isempty(obj.cm) && det(K_ef)>.0001
                C = inv(K_ef);
                Cp = [C(1,1) C(1,2); C(2,1) C(2,2)] + obj.cm*[-C(1,5)
C(1,4); -C(2,5) C(2,4)];
                obj.Lambda = max(eig(Cp));
            else
                obj.Lambda = NaN;
            end
        end

        function  kef = Kef3D(obj,u,k,t,l,r)
        %Kef3D Finds 6x6 stiffness matrix of end effector
        %   Detailed explanation goes here
            kef = (k-t/l)*[u*u', u*u'*obj.skew(r)'; obj.skew(r)*u*u',
obj.skew(r)*u*u'*obj.skew(r)'] ...
                + (t/l)*[[1,0,0;0,1,0;0,0,1], obj.skew(r)';obj.skew(r),
obj.skew(r)*obj.skew(r)']...
                + t*[zeros(3,6);zeros(3,3), obj.skew(u)*obj.skew(r)];
        end

        function  M = skew(obj,r)
        %Skew Matrix
        %   input 1x3 vecotr outpu 3x3 matrix
```

```
            M = [ 0 -r(3) r(2)
                  r(3) 0 -r(1)
                  -r(2) r(1) 0];
        end

    end
end
```

PerformancePlots.m

This code uses SkyBAAM.m and plots the performance of SkyBAAM across the workspace.

```
clc
clear
close all
load('calibration.m','-mat')
R = [12 0 52
    12 -12 16
    12 12 16
    0 12 52
    0 12 16
    0 0 39.5
    -12 0 31.25
    0 -12 31.25]';

bot = SkyBAAM(R,G);
bot.CableWeights = .029*ones(1,8)/12;
bot.CableDiameters = (1/8)*ones(1,8);
bot.setWeight(130);
bot.cm = 26;

%Set evaluation points
xmax = 200;
xmin = -200;
ymax = 200;
ymin = -200;
zmin = -100;
zmax = 200;
step = 10;
zstep = 50;
Z = zmin:zstep:zmax;
X = xmin:step:xmax;
Y = ymin:step:ymax;
[X,Y,Z] = meshgrid(X,Y,Z);
len = prod(size(X));

for i = 1:len
    x(i)=X(i);
    y(i)=Y(i);
    z(i)=Z(i);
    bot.SetPose([x(i);y(i);z(i)]);
    tol=.9;
    bot.SelectT(tol);
    if det(bot.Jacobian([1,4,6],1:3))>.5 && bot.TensionMargin>.2
        xTen(i) = bot.CableTensions(7);
        yTen(i) = bot.CableTensions(8);
        xMotion(i) = sum(bot.CableTensions(1:3));
        yMotion(i) = sum(bot.CableTensions(4:5));
        zMotion(i) = bot.CableTensions(6);
        L(i) = bot.Lambda;
```

```
        xminT(i) = bot.x_min_Tension;
        yminT(i) = bot.y_min_Tension;
    else
        xTen(i)=NaN;
        yTen(i)=NaN;
        L(i)=NaN;
        xMotion(i) = NaN;
        yMotion(i) = NaN;
        zMotion(i) = NaN;
        xminT(i) = NaN;
        yminT(i) = NaN;
    end
%     V(i) = 0;
%     W(i) = 0;
    S(i)=20;
end

scatter3(x,y,z,S,xTen,'filled')
c=colorbar;
title('X Prime Station Tension')
c.Label.String = 'Tensions (lbs)';
camorbit(5,-12)
xlabel('x (in)')
ylabel('y (in)')
zlabel('z (in)')

figure
histogram(xTen)
xlabel('X Prime Tension (lbf)')
ylabel('Number of Instances')

figure
scatter3(x,y,z,S,yTen,'filled')
c=colorbar;
title('Y Prime Station Tension')
c.Label.String = 'Tensions (lbs)';
camorbit(5,-12)
xlabel('x (in)')
ylabel('y (in)')
zlabel('z (in)')

figure
histogram(yTen)
xlabel('Y Prime Tension (lbf)')
ylabel('Number of Instances')

figure
scatter3(x,y,z,S,xMotion,'filled')
title('X Station Tension')
c=colorbar;
c.Label.String = 'Tensions (lbs)';
camorbit(5,-12)
xlabel('x (in)')
```

```
ylabel('y (in)')
zlabel('z (in)')

figure
scatter3(x,y,z,S,yMotion,'filled')
title('Y Station Tension')
c=colorbar;
c.Label.String = 'Tensions (lbs)';
camorbit(5,-12)
xlabel('x (in)')
ylabel('y (in)')
zlabel('z (in)')

figure
scatter3(x,y,z,S,zMotion,'filled')
title('Z Station Tension')
c=colorbar;
c.Label.String = 'Tensions (lbs)';
camorbit(5,-12)
xlabel('x (in)')
ylabel('y (in)')
zlabel('z (in)')

figure
scatter3(x,y,z,S,L,'filled')
c=colorbar;
c.Label.String = '\lambda_1';
camorbit(5,-12)
xlabel('x (in)')
ylabel('y (in)')
zlabel('z (in)')

figure
histogram(L)
xlabel('\lambda_1 (lb/in)')
ylabel('Number of Instances')

figure
scatter3(x,y,z,S,xminT,'filled')
c=colorbar;
c.Label.String = 'xmin';
camorbit(5,-12)
xlabel('x (in)')
ylabel('y (in)')
zlabel('z (in)')

figure
scatter3(x,y,z,S,yminT,'filled')
c=colorbar;
c.Label.String = 'ymin';
camorbit(5,-12)
xlabel('x (in)')
ylabel('y (in)')
```

```
zlabel('z (in)')
```

Workspace.m

This code plots the boundary of the SkyBAAM workspace.

```
clc
clear
%close all
load('calibration.m','-mat')

global bot
global theta
global phi
bot = SkyBAAM(R,G);
bot.CableWeights = .029*ones(1,8)/12;
bot.CableDiameters = (1/8)*ones(1,8);
bot.setWeight(130);
radius = 330;

Theta = 0:.3:2*pi-.01;
Phi = 0.01:.3:pi-.01;
X=[];
Y=[];
Z=[];
R=100;
WAIT = waitbar(0);
for i = 1:length(Theta)
    for j = 1:length(Phi)
        theta=Theta(i);
        phi=Phi(j);
        r_range = [1 2*max(max(G))];

        %Find edge of workspace
        for k = 1:10
            O = [objective(r_range(1)) objective(mean(r_range))
objective(r_range(2))];
            if sign(O(1))==sign(O(2)) && sign(O(2))~=sign(O(3))
                r_range(1)=mean(r_range);
            elseif sign(O(2))==sign(O(3)) && sign(O(1))~=sign(O(2))
                r_range(2)=mean(r_range);
            elseif sign(O(1))<0 && sign(O(1))<0 && sign(O(1))<0
                r_range = [max(max(G)) max(max(G))];
                break
            else
                r_range = [0 0 ];
                break
            end
        end
        R = mean(r_range);


        p = [R*cos(theta)*sin(phi), R*sin(theta)*sin(phi), R*cos(phi)];


        %max(bot.CableTensions)
```

```
        X = [X p(1)];
        Y = [Y p(2)];
        Z = [Z p(3)];
    end
    WAIT = waitbar((i-1)/length(Theta));
end

WAIT = waitbar(1);


%% Plot

c = [1 2 12; 2 3 13; 3 4 14;4 5 15;5 6 16; 6 7 17;7 8 18;8 9 19;9 10
20;10 11 21;13 2 12; 14 3 13; 15 4 14;16 5 15;17 6 16; 18 7 17;19 8
18;20 9 19;21 10 20;22 11 21];
C=c;
for i=1:length(Theta)-1
  C = [C;[c+11*i]]; %conectivity
end
for i=1:1260
   if C(i)>length(X)
       C(i)=C(i)-231;
   end
end


bot.SetPose([0;0;0]);
bot.show;
plot3(G(1,:),G(2,:),G(3,:),'r*')
hold on
%plot3(X,Y,Z,'.')
hold on
tri = triangulation(C, X',Y',Z');
trisurf(tri)

close(WAIT)

xlabel('x (in.)')
ylabel('y (in.)')
zlabel('z (in.)')
%zlim([-100,300]);
grid on

%%

function val = objective(r)
    r=abs(r);
    global bot
    global theta
    global phi
    p = [r*cos(theta)*sin(phi), r*sin(theta)*sin(phi), r*cos(phi)];
    bot.SetPose(p);
```

```
    bot.SelectT(.9);
    if bot.TensionMargin>.2 &&  det(bot.Jacobian([1,4,6],1:3))>.5 %&&
max(bot.CableTensions([7,8]))<300
        val = -r;
    else
        val = r;
    end

end
```

VITA

Phillip Chesser is a native of Knoxville, Tennessee. He received his undergraduate degree in mechanical engineering from Tennessee Technological University in the Spring of 2016 with a 4.0 GPA, having been an officer in the university chapter of both Tau Beta Pi and Pi Tau Sigma. He went on to take a post-bachelor position and then a researcher position at Oak Ridge National Laboratory at the Manufacturing Demonstration Facility where he performs research primarily on large-scale additive manufacturing. In his work there he has helped develop many additive manufacturing systems, led design for additive manufacturing for a printed nuclear reactor, consulted and worked with industry partners, and authored many publications. He has authored or co-authored over 20 peer review publications with over 140 citations, many technical reports, and has 3 granted patents with several more that are pending. His research at Oak Ridge National Laboratory led him to pursue a Master of Science degree in mechanical engineering from the University of Tennessee, where he will graduate in the Spring of 2021. In his spare time, he enjoys hiking and other outdoor activities, and spending time with friends and family.